**Carderock Division**
**Naval Surface Warfare Center**
Bethesda, MD 20084-5000

(2)



**CARDEROCKDIV-SME-92/22** April 1992
Ship Materials Engineering Department
Research and Development Report

# Effect of Assembly Anomalies on the Strain Response of Composites in the Sphere Joint Region of the DARPA Man-Rated Demonstration Article

by
E.T. Camponeschi, Jr.[1]
R.E. Bohlmann[2]
J. Hall[3]
Ens. T.T. Carr, USN[1]



[1]CARDEROCKDIV, NSWC
[2]McDonnell Aircraft Co.
[3]General Dynamics, EB Div.



Effect of Assembly Anomalies on the Strain Response of Composites in the Sphere Joint Region of the DARPA Man-Rated Demonstration Article
CARDEROCKDIV-SME-92/22

**Carderock Division**
**Naval Surface Warfare Center**
Bethesda, MD 20084-5000

**CARDEROCKDIV-SME-92/22** April 1992
Ship Materials Engineering Department
Research and Development Report

# Effect of Assembly Anomalies on the Strain Response of Composites in the Sphere Joint Region of the DARPA Man-Rated Demonstration Article

by
E.T. Camponeschi, Jr.[1]
R.E. Bohlmann[2]
J. Hall[3]
Ens. T.T. Carr, USN[1]

[1]CARDEROCKDIV, NSWC
[2]McDonnell Aircraft Co.
[3]General Dynamics, EB Div.



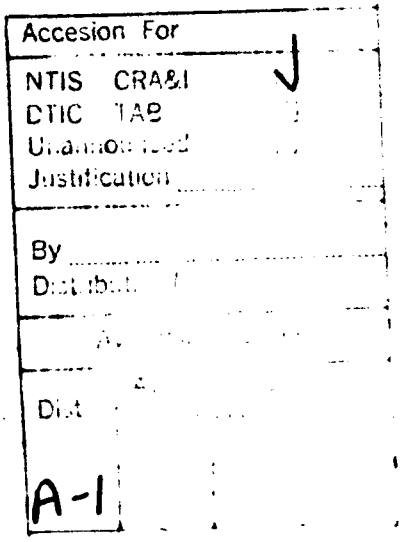

## Table of Contents

## List of Tables



## List of Figures

## Abstract

*The compressive response of thick, quasi-isotropic, AS4/3501-6 laminates with geometric anomalies were investigated theoretically and experimentally. The specimens considered were rectilinear with nominal dimensions of 10 inches long, by 4 inches wide, by 0.78 inches thick. The anomalies were designed to simulate expected fit-up clearance conditions resulting from normal manufacturing tolerances in the sphere joint regions of the DARPA Man Rated Demonstration Article. Tests were conducted both with unfilled fit-up gaps and with fit-up gaps filled with a polymer shimming material (Hysol EA9394). Strains were monitored in the specimen gage sections and in regions of high strain concentration resulting from the manufacturing anomalies. Measured strains correlated well with predicted strains from an ABAQUS Finite Element Analysis. For all test cases the specimens were able to withstand strains due to the anomalies when gage section strain reached 7000 microstrain. One specimen with no anomalies was tested to failure in uniaxial compression and failed in the gage section at 89,000 psi and 13,500 microstrain, which is equivalent to thin-section composite failure strains.*

## Administrative Information

This program was supported by Mr. Jim Kelly, the Program Area Manager for Materials of the DARPA AST program, under work unit 1-2802-304.

## Introduction

The information discussed in this report pertains to the DARPA AST program and in particular to the application of fiber-reinforced composite materials to the Man Rated Demonstration Article (MRDA) [1, 2]. The MRDA is comprised of a cylindrical hangar section, a spherical access chamber, a spherical hyperbaric chamber and a modular end-dome (Fig. 1). These components are joined to form a single structure, and the joints in the spherical elements are designed of titanium. The stress state in the regions where the titanium and composite material is in contact are very complex. Finite element analysis of the joint region of the composite spheres indicate that small changes in manufacturing tolerances create significant concentration of strain in the composite spherical hyperbaric chamber. In this region strains have been shown to be particularly high in the sphere at the point where it contacts the titanium joint. The joint region

of concern is shown in Fig. 2.

The tolerance variables considered in this investigation were the thickness of the fiberglass tabs and the perpendicularity between the composite sphere tabs and the composite sphere ends. Since the fiberglass tabs were to serve as sacrificial material to be machined for fit-up between the sphere and joint, two possible machining conditions were considered. The first was to have equal amounts of fiberglass (0.060 inches) on each side of the composite sphere from a symmetric machining operation. The second was to have all machining performed on the inside of the sphere resulting in full tab thickness on the outside of the sphere (approx. 0.120 inches) and essentially no tab material left on the inside.

The second tolerance condition, out-of-perpendicularity between the sphere end and joint, may result from machining or fit-up would occur where the end of the sphere seats in the titanium joint. For the best case condition the entire end of the sphere would contact the joint with no clearance in the fit. With the spherical geometry and size of both components there is the possibility of a clearance in this region rather than intimate contact. To simulate both tolerance conditions, a series of rectilinear coupons to be loaded in uniaxial compression were machined as summarized in Figs. 3 and 4.

In order to quantify the effects of these two manufacturing conditions a set of uniaxial joint compression tests were outlined. These tests would not simulate identically the triaxial state of stress present in the actual sphere joint assembly under hydrostatic pressure, but would quantify the magnitude and effect of the strain concentration caused by the manufacturing conditions. Specifically the magnitude of longitudinal strain at the base of the composite specimen would be compared to the magnitude of strain in the gage region of the specimen in the presence of fit-up gaps and for perfect fit-up conditions. These specimens would also be inspected for evidence of local failure or damage in the regions of high strain.

The test plan for this investigation is detailed in Figs. 3 and 4. This plan calls for the testing of 9 specimens, 3 tested with no manufacturing anomalies and 6 with varying anomalies. Of the 6 with anomalies, 3 cases contained liquid shim (Hysol EA 9394) in the areas where fit-up gaps were present and 3 cases were conducted with bare fit-up gaps.

The test plan called for the following procedure for all of the tests:

1) Load the specimen to the point when the gage section reached a compressive strain of 6700 microstrain,
2) Hold the load on the specimen for 5 minutes,
3) Unload the specimen
4) Record load and seven channels of strain for all tests.

## Sphere and Test Specimen Analysis

General Dynamics/Electric Boat Division performed numerous ABAQUS 2-D plane strain finite element analyses of the sphere joint test configurations prior to testing in order to predict the strain levels under loading. The finite element mesh and material properties used are shown in Fig. 5 and Table 1 respectively. The four experimental test cases modeled with the finite element program ABAQUS are listed in Table 2. Although these models do not match exactly the pad-up sizes in the actual tests, they are sufficiently similar to the test configuration of Fig. 4 to allow valid comparisons of the predicted strain and the experimentally measured strain.

## Specimen Fabrication and Preparation

Thermoset composite compression specimens, 0.78" thick, were fabricated by McDonnell Aircraft Co. St Louis, MO (McAir) and delivered to DTRC for testing. These specimens are representative in geometry and material of the modular composite sphere joint in the MRDA. They were fabricated per McAir Engineering Drawing MRDVTST1 "Test Specimens Sphere Pad-Ups."

The composite laminates used to simulate sphere geometry were made of AS4-3501-6 unidirectional net resin 10 mil prepreg. The tabs bonded to the laminate were made of 7781 Glass/Epoxy F-161 fabric material, having an I-550 finish and were used to simulate sphere pad-ups. The adhesive used to bond the tabs to the compression specimen laminates was FM-300 film adhesive.

### Carbon/Epoxy Compression Specimen Fabrication

The compression specimens were fabricated from a 48" x 16" flat panel layed up from AS4 / 3501-6 unidirectional prepreg. The ply orientation was

$[(\pm 45, 0, 90)_9 / (0,\overline{90})]_s$ resulting in a 0.78" thick panel. Due to the extensive number of plies, a chisel cutter was used to accelerate ply cutting. The plies were hand layed up and vacuum debulked every ten plies. The project plate and caul plate used for part fabrication were release coated with Frekote 44 for easy part removal. Fig. 6 shows the bagging sequence used during cure of the panel.

After assembly and vacuum bagging, the panel was autoclave cured at 250°F and 100 psi for 2 hours and post cured at 350°F, 100 psi for 4 hours. Nondestructive evaluation (C-Scan) of the panel showed good consolidation.

The areas of the compression specimens that were to have end tabs bonded on them were cleaned and prepared for bonding by scuff sanding with 220 grit sandpaper. Next the panel was dried in an oven at 200°F for 2 hours to remove any moisture. Two aluminum tools (Fig. 7) were made and release coated with Frekote 44 for cobonding the fiberglass end tabs to the carbon/epoxy laminate. The FM-300 film adhesive was B-staged in an oven at 240°F for 20-30 minutes to remove any volatiles and to reduce flow during cobonding.

Cobonding of Fiberglass End Tabs

The fiberglass/epoxy cloth of the two end tabs was hand layed up into $[\pm 45]_{26}$ and $[\pm 45]_{13}$ laminate configurations. The ply stacks were pre-bled prior to cure at 185°F for 30 minutes. The plies going on the lower side of the panel were placed directly into the tool and the other half were placed on the cured carbon/epoxy panel. One ply of the FM-300 adhesive was sandwiched between the panel and end tabs during assembly. The assembly (Fig. 7) was cured in an oven under vacuum pressure at 300°F for 4 hours.

The compression specimens fabricated from this panel were made to fulfill the requirements of the test matrix shown in Fig. 3. The end tab geometry varied slightly for each of the 7 different test cases so they were machined to the required geometry. The individual specimen geometries and tolerances are included in the Appendix A.

End Tab Quality

The quality of the quasi-isotropic AS4/3501-6 autoclave cured flat laminate was excellent as determined by Ultrasonic C-Scan and photomicroscropy, Fig. 8. The fiberglass fabric prepreg end tabs (±45 degree

layup) and FM-300 adhesive were cured (300°F, vacuum bag) to the precured AS4/3501-6 laminate as previously discussed. The microstructure of the end tab region is shown in Fig. 8. Since only vacuum bag pressure was used during cure, the end tabs have a high void content (~10%). A compression strength test was conducted on a ±45 degree fabric layup with similar void levels and a failure strain of >21,000 microstrain was achieved (Fig. 9). This strain level is significantly higher then the design requirement for the joint (~ 7,000 microstrain) and therefore the tab quality is acceptable.

## Description of Test Method and Test Plan

The tests to be performed in this investigation were essentially uniaxial compression test on thick composite materials. The design for the test fixture was dictated by the geometry and dimensions of the MRDA half-scale sphere joint. The actual joint geometry is not symmetric about the specimen midplane, but the joint test fixture was designed symmetric about the specimen midplane to reduce the complexity of the test setup and eliminate test variables. A schematic of the final joint test fixture is shown in Fig. 10.

The width of the test fixture was selected to be 4 inches. This was the smallest dimension that allowed two bolts to be used to clamp the fixture together while maintaining the sub-scale bolt centers (2.94 inches). Other dimensions were selected to match those of the MRDA sub scale sphere joint. Since the bolt size and spacings were designed for a full row of bolts in the actual sphere joint, a stress analysis was performed for the two bolts to be used in the joint test fixture. The same bolt specification for the sphere joint assembly (1/2-13 UNC) was used for the joint fixture. Bolt stress was estimated from the following equation [3]:

$$\frac{\sigma_b}{\sigma_x} = \frac{\nu_{xx}}{E_x}\left[\frac{E_b E_z A_c t}{L_b E_z A_c + E_b A_t t}\right] \qquad (1)$$

where:

$A_t$ = total bolt cross-sectional area,

$A_C$ = surface area of contact between one tab and fixture,

$E_b$ = bolt modulus,

$E_x$, $E_z$ = specimen longitudinal and through-thickness modulus,
$L_b$ = bolt length,
t = total thickness of specimen and tabs,
$\nu_{xz}$ = through-thickness Poisson's ratio,
$\sigma_b$ = bolt stress, and
$\sigma_x$ = longitudinal stress in laminate

Specimen length was selected to allow full design length fiberglass tabs on both ends of the specimen and a nominal 1.0 inch specimen gage length. The joint fixtures to be used in the compression tests did not have a very large "footprint" on the test machine crossheads and was not mechanically attached to them, raising concern over the stability of the 10 inch long specimen and fixtures. Using the classical Euler buckling equation, buckling loads for the specimens were calculated assuming both pinned ($P_{cr} = \pi^2 E_x I / L^2$) and clamped end conditions ($P_{cr} = 4 \pi^2 E_x I / L^2$) ($E_x$ = longitudinal modulus, I = moment of inertia, L = specimen length). The results showed that the load planned for the tests (150,000 lbs.) fell between the buckling load for the pinned condition (110,000 lbs.) and the buckling load for the clamped condition (437,000 lbs.)

Since the actual end conditions were somewhere between these two conditions and specimens with end bevels would cause severe load eccentricities, an auxiliary fixture base was designed to provide greater global stability. This auxiliary fixture was steel and designed to clamp firmly to the titanium fixture after the specimen was bolted into the titanium fixture (Fig. 10). The auxiliary fixture provided more fixture stability by providing a larger area of contact on the test machine crossheads than provided by the titanium fixture alone. No instability problems were encountered during any of the joint tests conducted. A photograph of the entire test assembly is shown in Fig. 11 and machine shop drawings for the joint test fixture and auxiliary fixture are included in Appendix B.

The compression tests were performed in a 300,000 lb. Tinius Olsen screw Driven load frame. Crosshead speed for all of the tests was 0.05 inches per minute.

## Instrumentation and Data Reduction

Strain data was recorded for each test case using 350 ohm CEA-06 type resistance strain gages. Seven unidirectional gages were mounted on each specimen. For specimens with square end conditions 0.125 in. or 0.250 in. gages were mounted on the specimens as shown in Figs. 12 and 13. For specimens with beveled end conditions 0.062 in. of 0.250 in. gages were mounted on the specimens as shown in Figs. 14 and 15. For the purposes of data reduction each gage was assigned a code to designate its location on the specimen as shown in these Figs.

Strain was monitored with multiple Micromeasurements 2310 conditioner amplifiers and recorded along with load using a DTRC written data acquisition program running on an IBM-AT computer. Corrections for Wheatstone bridge nonlinearities were automatically made in the data acquisition program although these errors should be insignificant for the strains recorded in this study.

The stress and strain data is recorded in spreadsheet format with the data acquisition system and is then plotted for inclusion in this report.

Stress to be plotted against strain in the gage section was computed by dividing far-field load by gage section cross-sectional area. The stress associated with the gages at the base of the specimen was calculated based on an "effective area" of the specimen in this region. The "effective area" was calculated by converting the end tab cross-sectional area to an "effective area" for carbon/epoxy end tabs with the same laminate modulus as the specimen. This conversion was performed using the following equation;

$$A_B = A_{C/E} + A_{F/E} \times \frac{E_{X\text{-}F/E}}{E_{X\text{-}C/E}} \qquad (2)$$

where:

$A_B$ = Effective cross-sectional area at the specimen base

$A_{C/E}$ = Cross-sectional area of the carbon/epoxy in the gage section

$A_{F/E}$ = Cross-sectional area of the fiberglass/epoxy

$E_{X\text{-}F/E}$ = Longitudinal modulus of the fiberglass/epoxy

$E_{X\text{-}C/E}$ = Longitudinal modulus of the carbon/epoxy

The effective cross-sectional area for all specimens except for the one

used in Test Case 2 is 3.511 square inches, versus 3.840 for the actual cross-sectional area at the base. These numbers are based on a the following values: $A_{C/E}$ = 3.360 sq. in., $A_{F/E}$ =0.480 sq. in., $E_{X\text{-}F/E}$ = 2.1 Msi and $E_{X\text{-}C/E}$ = 6.67 Msi.

## Results and Discussion

Finite Element Analysis Results

The four experimental test cases modeled with the finite element program ABAQUS are listed in Table 2 and were Test Case 1 (Baseline), Test Case 3 (0.020 end bevel), Test case 4 (0.040 end bevel), and Test Case 8 (0.02 end bevel and liquid shim). For each model the specimen was loaded to 25,000 psi in the gage section and the resulting strain was compared to the strain measured in the corresponding compression test. The results from the finite element analysis are summarized in Table 3. These results show that with the exception of the bottom strain gages in Test Case 8 (0.02 end bevel and liquid shim), the experimental results were within the range of the theoretical results or within 8% of the range of the theoretical results for all of the test cases analyzed. These results are highly acceptable considering the strain gradient predicted by the finite element analysis and the the fact that strain gage results yield average results in the presence of a strain gradient.

For the bottom gages in Test Case 8 the theoretical results were 30-40% higher than the experimental results. The experimental strain gage results from this test seem unusually low, but the bottom strain gage results from Test Cases 6 and 7 were for similar conditions and were similarly low. The reason for these low strains has not been determined precisely but it is most likely due to the combination of 1) load sharing that occurs along the flanges of the test fixture and 2) the non uniform load distribution across the width of the specimen at its base. This issue is discussed below for the Baseline specimen test results, but the load distribution at the specimen base is expected to be more non uniform in the presence of the liquid shim (which plastically deformed) than for the baseline specimens. A schematic of uniform base loading and possible non uniform load distributions is shown in Fig. 16.

Based upon the above results and discussion, the mesh size, assumed material properties, and strain results from the ABAQUS FEM are

considered adequate for predicting the longitudinal compressive strain response in the design operating envelope for the composite sphere ends.

Baseline Specimens (Test Cases 1A and 1B)

The stress-strain plots for the two baseline test specimens (Test Case 1A and 1B) are shown in Figs. 17 and 18. All strains on the composite specimen and on the titanium fixture were compressive. The compressive strain at the root of the fixture flange resulted from bending of this flange due to Poisson expansion of the composite specimen under compressive load. This strain was negligible (< 2000 microstrain) for this and all follow on test cases and indicates the design thickness of the joint flanges is adequate for all possible manufacturing conditions of the sphere joint.

The longitudinal compressive strain in the specimen gage section are shown in the righthand most curves of Figs. 17 and 18. For both tests the four strain readings were essentially identical indicating no bending in either the x-z or y-z plane of the specimen. The drift in strain seen in the front edge gage (EF) in test 1A was traced to incorrect shunt calibration resistors in the strain gage conditioner-amplifier and was corrected for test case 1B.

The middle two curves in Figs. 17 and 18 were from the gages on the bottom of the test specimen (BF and BB). Even with the correction for the effective area in the base of the specimens the bottom gages report lower strains than the gage section gages. This can be attributed to two factors, 1) that some of the compressive stress into the gage section is transferred via shear from the flanges on the joint fixture and 2) the end load at the base of the specimen is not distributed uniformly across the width of the specimen. For the second factor more of the load may be transferred at the middle of specimen width than at the edges where strain is being measured (Fig. 16). This is not the case in the gage section of the specimen where strains on the faces and edges of the specimens are equal. The actual strain (load) distribution across the specimen width was not determined. These two factors combined, appear to account for approximately 10-15% of the total load transfer.

Specimen With Maximum End Tab Thickness (Test Case 2)

The stress strain plot for this specimen is shown in Fig. 19. The major

observation from this plot is that the strain readings on the faces of this specimen appear to be diverging with increasing load. This strain response is indicative of global specimen bending that would be expected for this specimen considering that there is essentially no tab material on one face of the specimen, and 0.120 inches of tab material on the other face. This condition creates a load eccentricity as shown in the free body diagram of Fig. 20. This figure also shows that the load eccentricity caused by the unequal tab thicknesses can be accounted for by considering the contributions of the moment in the gage section due to the eccentricity. When accounted for, the face strain readings are predicted as 5,316 μ in/in (FL) and 7.877 μ in/in (FR) compared to the measured strains at 44,000 psi of 4,900 μ in/in (FL) and 8,000 μ in/in (FR).

Specimens With End Bevels (Test Cases 3 and 4)

The stress strain plots in Figs. 21 and 22 are for the the two test cases with end bevels on the specimens and no liquid shim material to fill the gap created by this end condition. For Test Case 3 (Fig. 21), the specimen with a 0.020 inch end bevel, the strain response in the specimen test section is essentially the same as for the baseline specimens. The change in strain response could be seen in the gages on the specimen edge near the specimen base (BFL, BFR, and BBL). The two gages on the base and in the corner where the specimen contacted the fixture (BBL, BFL) showed an extreme nonlinearity and rapid strain increase during initial loading. This condition changed between 10,000 and 20,000 psi, where relatively linear stress strain response at the same slope as the baseline specimens continued. Although not conclusively demonstrated, it is speculated that most of the base of the specimen was in contact with the fixture when the response of the base gages became linear. Since the slope of this response is lower at the base than in the gage section, and since the response became linear early in the loading curve, the strain in the base of the specimen was lower than that in the gage section at 48,000 psi. Of course any strain gage reading is an average value, and localized strain right at the specimen base is unknown. No visible damage was observed on the base of the specimen after this loading cycle.

For Test Case 4 (Fig. 17), the specimen with a 0.040 inch end bevel, the divergence of the strain response in the test section shows bending of the

test specimen. This bending was not leading to global instability at 40,000 psi since the response was still essentially linear at this stress level. The gages near the bottom of the specimen showed the same basic trend as for the previous test case; rapidly increasing strain in the gages near the contact region, and slowly increasing strain in the gages on the edge with the gap. The primary change in the strain response from the 0.020 gap case is the strain response in the base gages changed from extemely nonlinear to relatively linear between 20,000 and 35,000 psi rather than between 10,000 and 20,000 psi.

To further investigate the strain nonlinearities observed in Test Cases 3 and 4 the unloading curves for the base gages were reviewed. These curves are shown in Figs. 23 and 24 and show the response was nonlinear-elastic.

Specimens With Liquid Shim (Test Cases 5-8)

Test Cases 5-8 were ones in which the gaps between the specimen and fixture were filled with liquid shim prior to testing. The strain response in Test Case 5 (Fig. 21, 0.020 inches of liquid shim between one tab and the fixture) was the same as for a baseline specimen as shown in Fig. 25.

Test Cases 6 and 7 showed base strain gage response quite different from that of the beveled specimen with no liquid shim (Test Case 3). Figs. 26 and 27 show that the gage section strain response of Test Case 6 and 7 was the same as for the baseline specimens.

The base gage strains for these two Test Cases were much lower than that for the same specimen with no liquid shim (Case 3) and were very nonlinear. The lower strain response of the base gages can most likely be attributed to the fact that the end load at the base of the specimen is not distributed uniformly across the width of the specimen, as shown in Fig. 16. Upon unloading and reloading the specimens from Case 6 and 7, Figs. 28 and 29, a different nonlinear response was observed. Although not shown in these figures, the ramp-up strain response from the second loading followed the ramp-down strain response seen when unloading the specimen in the first test. The response observed for these test cases suggest plastic deformation of the liquid shim occurred between 10,000 and 20,000 psi. Significant plastic flow of the cured shim was observed after the completion of the two loadings for Text Case 7, and is shown in Fig. 30. Strain response upon subsequent reloadings of Test Cases 6 and 7 is

expected to be the same as the second loading but this was not experimentally demonstrated.

Test Case 8 was not in the original test plan but was added to investigate the sensitivity of the liquid shim to repeated loadings at design operating strain levels. The geometric details of this Case are shown in Fig. 4, and the specimen was loaded to 2000 microstrain and unloaded 10 times at a crosshead displacement rate of 0.05 inches per minute. Plastic deformation of the liquid shim did not occur at or below 2000 microstrain by nature of the linear and repeatable strain response for the ten cycles to this strain level, Fig. 31. As with Test Cases 6 and 7 when the specimen for Test Case 8 was loaded to 2000 microstrain in the test section the base gage response was very nonlinear above 20,000 psi (Fig. 32) due to plastic deformation of the liquid shim. Fig. 33 shows a stress-strain curve to 7000 microstrain after plastic deformation of the liquid shim.

Baseline Specimen Test to Failure (Test Case 9)

After completion of the test program summarized above one baseline test specimen was loaded to failure using the same fixturing as above. Failure occurred instantly and in the center of the gage section at a stress level of 89,000 psi and at an average strain of 13,500 microstrain. A photograph of the specimen after failure is included in Fig. 34. These results were considered excellent for a thick compression strength test and were the same as expected from a standard thin section compression test of the same type material and layup. The strain response for this test is shown in Fig. 35 and showed excellent specimen stability up to failure with only slight divergence of the two gages on the faces of the laminate.

Significant nonlinearity in the longitudinal modulus of this specimen was observed with a chord modulus of 6.80 Msi between 1000 and 3000 microstrain and 5.39 Msi between 11,900 microstrain and failure (13,900 microstrain). This is a drop in modulus of 20.7 % and these results are summarized in Table 4.

Titanium Fixture Response

The strain response of the titianium fixtures was investigated with strain gages located on the root of the fixture flange (Fig. 12). As seen in the stress-strain curves for all 9 of the test cases described above, the strain at

the root of the fixture flange never reached a value greater than 2000 με other than for Test Case 4 with the 0.040 unfilled bevel. In this case the titanium strain reached 4000 με at the test condition of 43,000 psi. In a test case where 3 strain gages were placed across the witdh of the titanium flange root, the strain distribution was shown to be consistent across the fixture width. Because of these results the design of the titanium joint for the MRDA sphere as represented in these tests is adequate.

## Conclusions

Based on the theoretical and experimental results of this program the following conclusions are drawn:

1) Based on the comparison of the theoretical and experimental strain results, the mesh size and assumed material properties used in the ABAQUS Finite Element Analysis are considered adequate for predicting the unidirectional, longitudinal compressive strain in thick laminates with end anomalies and rigid bearing surfaces. In the presence of compliant bearing surfaces (as with liquid shim), theoretical strain predictions can vary significantly from experimental results. Theoretical and experimental comparison of stress analysis methods for the actual sphere joint geometry of the MRDA, with its associated 3D stress state have not been addressed in this study.
2) The gaps that may occur between the composite sphere and titanium joints due to manufacturing tolerances do not create stress concentrations that will adversely affect the response of the sphere or joint under normal design operating loads.
3) The quasi-isotropic carbon epoxy material tested in the study was able to withstand the state of stress (strain) created by the manufacturing anomalies created in the test specimens. No local failure was evident as a result of the specimen end bevels that created near line contact compressive loads on the specimens.
4) Based on the strain measured at the base of the titanium fixture flanges, the design thickness of these flanges is adequate for all possible manufacturing conditions of the sphere joint.
5) Hysol EA9394, liquid shimming material, when used to fill manufacturing fit-up gaps, distributes load and reduces the stress

concentration that results from the gap; however, the liquid shim, when allowed to deform freely, undergoes significant plastic deformation at compressive loads of approximately 20,000 psi and above.

6) Under uniaxial compressive loading, the tapered design of the titanium flanges has been shown to minimize the stress concentrations due to joint restraint where the composite exits the joint. This design serves to prevent premature specimen failures that would occur in the presence of such stress concentrations. The effect of this tapered flange design is expected to be the same for the actual MRDA joint geometry where 3D stresses will develop.

7) As a result of the fixture design discussed in conclusion 6, the results of the uniaxial compression test to failure are considered excellent for a thick composite compression strength test, and are the same as expected from a conventional thin section compression test of the same material type and layup.

## References


1. Hoffman, P. and Kelly, J. J., "Manufacture of Advanced Composite Submarine Structures (MACSS)," Proc. 37th International SAMPE Symposium, March 1992.

2. Leon, G. F. and Coffenberry, B., "Proposed Fabrication Processes for Thick Composite Submarine Structures," Proc. 37th International SAMPE Symposium, March 1992.

3. Camponeschi, E. T., Jr., "Compression Response of Thick-Section Composite Materials," David Taylor Research Report No. DTRC SME-90/60, October 1990.

Table 1. Material Properties Used in the Finite Element Analysis.

| Lamina Properties | Quasi-Isotropic Laminate Properties $[0/45/-45/90]_{ns}$ |
|---|---|
| $E_1$=15.4 Msi | $E_z$=2.11 Msi |
| $E_2$=1.65 Msi | $E_x$=6.27 Msi |
| $E_3$=1.65 Msi | $E_y$=6.27 Msi |
| $\nu_{12}$=.33 | $\nu_{xy}$=.32 |
| $\nu_{13}$=.33 | $\nu_{xz}$=.37 |
| $\nu_{23}$=.54 | $\nu_{yz}$=.37 |
| $G_{12}$=0.72 Msi | $G_{xy}$=0.238 Msi |
| $G_{13}$=0.72 Msi | $G_{xz}$=0.624 Msi |
| $G_{23}$=0.55 Msi | $G_{yz}$=0.624 Msi |

Table 2. Test Cases Modeled with the Finite Element Analysis.

| ABAQUS Model | Description |
|---|---|
| REV 17 | Baseline with 0.09 Inch Pad-Ups Each Side, Test Case 1A, 1B |
| REV 23A | Model 17 with 0.02 Inch Gap on Right-hand Side, Test Case 3 |
| REV 21A | Model 17 with 0.04 Inch Gap on Right-hand Side, Test Case 4 |
| REV 23B | Model 17 with 0.02 Inch Gap on Right-hand Side and Liquid Shim, Test Case 8 |

Table 3. Summary of Finite Element Analysis Results.

| | Longitudinal Strain Micro inches/Inch | | | | | | | |
|---|---|---|---|---|---|---|---|---|
| Gage Location | Middle | | | | Bottom | | | |
| Test Specimen | Finite Element Model | | Test | | Finite Element Model | | Test | |
| Baseline FEM-Rev 17 Test Case 1A,B | -3270 to -3370 | | -3640 (+8.0%)[1] | | -3060 to -3160 | | -2890 (-5.6%) | |
| | Left | Right | Left | Right | Left | Right | Left | Right |
| FEM-Rev 23A 0.02 Inch Gap Test Case 3 | -3530 to -4820 | -2240 to -3530 | -4030 (w) | -3430 (w) | -3530 to -6210 | +350 to -2240 | -3280 (w) | -750 (w) |
| FEM-Rev 21A 0.04 Inch Gap Test Case 4 | -3730 to -5730 | -1730 to -3730 | -4480 (w) | -2820 (w) | -3730 to -7730 | +200 to -1730 | -6210 (w) | -280 (w) |
| FEM-Rev 23A 0.02 InchGap Test Case 8 | -3250 to -3380 | -3250 to -3380 | -3520 (+4.0%) | -3410 (+1.0%) | -3110 to -3380 | -3250 to -3520 | -2130 (-31%) | -1710 (-47%) |

[1] - percent difference from Finite Element result, w = within the strain range predicted by the FEA

Table 4. Longitudinal Modulus Nonlinearity From Edge Mounted Strain Gages.

| Longitudinal Modulus Nonlinearity From Edge Mounted Strain Gages | | | |
|---|---|---|---|
| Edge Front Strain | Gage Section Stress | Edge Back Strain | Gage Section Stress |
| 996.6 με | 7029 psi | 991.3 με | 8144 psi |
| 3023 με | 20732 psi | 2987 με | 21781 psi |
| Initial Modulus = 6.76 Msi | | Initial Modulus = 6.83 Msi | |
| 11970 με | 78311 psi | 11680 με | 78042 psi |
| 13960 με | 88987 psi | 13700 με | 88987 psi |
| Final Modulus = 5.36 Msi | | Final Modulus = 5.42 Msi | |
| Average Initial Modulus = 6.80 Msi | | | |
| Average Final Modulus = 5.39 Msi | | | |
| Change in Average Modulus = - 20.7% | | | |

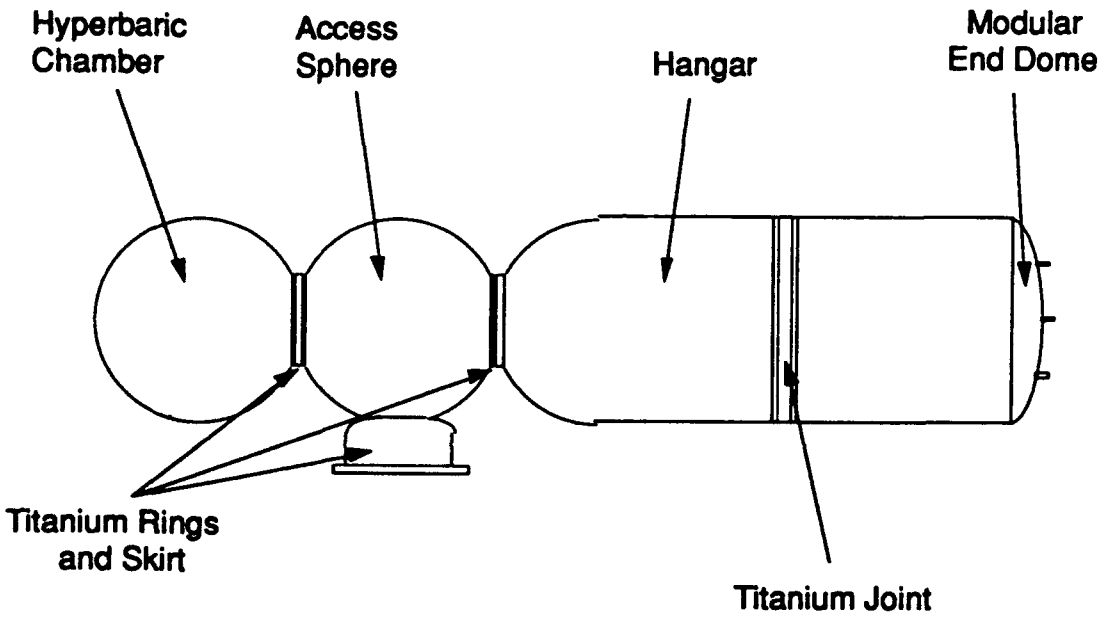


**Figure 1. MRDA Configuration**

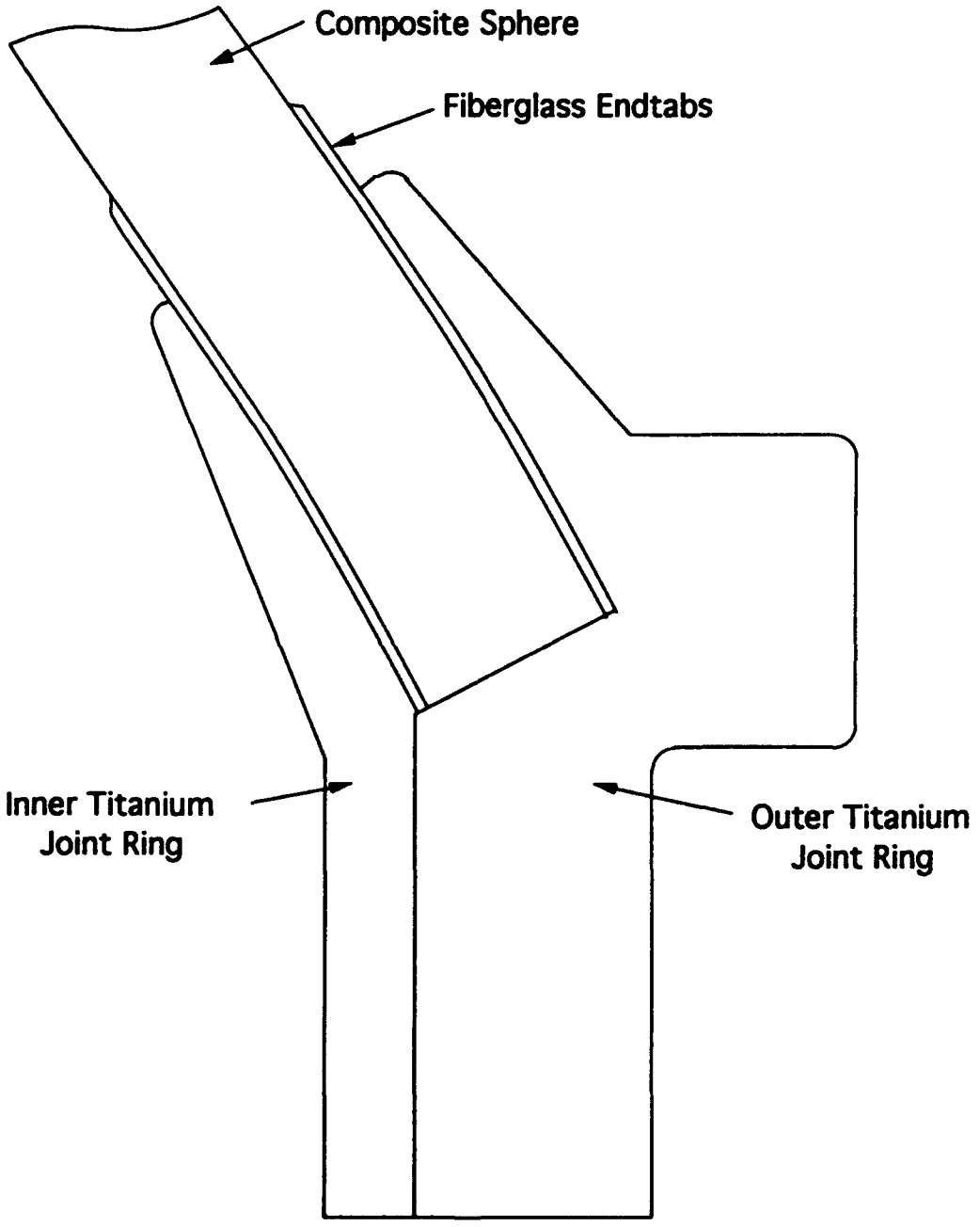


**Figure 2. Cross-Sectional View of the Modular Composite Sphere Joint in the MRDA.**

## Sphere Joint Test Matrix

- Test RT/as Received Moisture
- Test 2 Spare Specimens

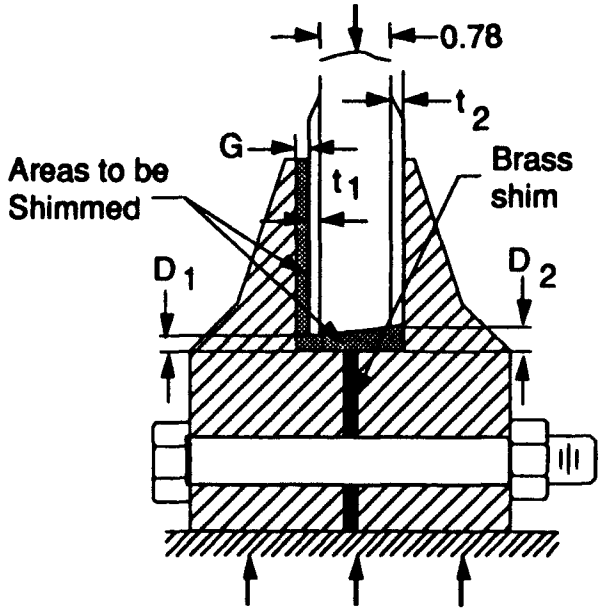


| Test Case | Evaluation Objective | Lateral Gap (G-in.) | Left Side Gap ($D_1$-in.) | Right Side Gap ($D_2$-in.) | End Tab Thickness t1 (in.) | End Tab Thickness t2 (in.) | End Shim | Spec. No. |
|---|---|---|---|---|---|---|---|---|
| 1A, B | Baseline, Nominal Case | 0 | 0 | 0 | 0.06 | 0.06 | No | 2003-2, 1 |
| 2 | Max. End Tab Thickness | 0 | 0 | 0 | 0.02 | 0.12 | No | 2005 |
| 3 | Effect of End Taper | 0 | 0 | 0.020 | 0.06 | 0.06 | No | 2007-1 |
| 4 | Effect of Severe End Taper | 0 | 0 | 0.040 | 0.06 | 0.06 | No | 2009 |
| 5 | Lateral Gap/Liquid Shim | 0.02 | 0 | 0 | 0.06 | 0.06 | No | 2003-3 |
| 6 | Lat. Gap/Taper/Liq. Shim | 0.02 | 0 | 0.020 | 0.06 | 0.06 | No | 2007-2 |
| 7 | End Taper and Liq. Shim | 0 | 0.06 | 0.080 | 0.06 | 0.06 | Yes | 2007-3 |
| 8 | End Taper and Liq. Shim | 0 | 0 | 0.020 | 0.06 | 0.06 | Yes | 2007-2 |
| 9 | Baseline, Test to Failure | 0 | 0 | 0 | 0.06 | 0.06 | No | 2003-3 |

Figure 3. Sphere Joint Test Matrix.

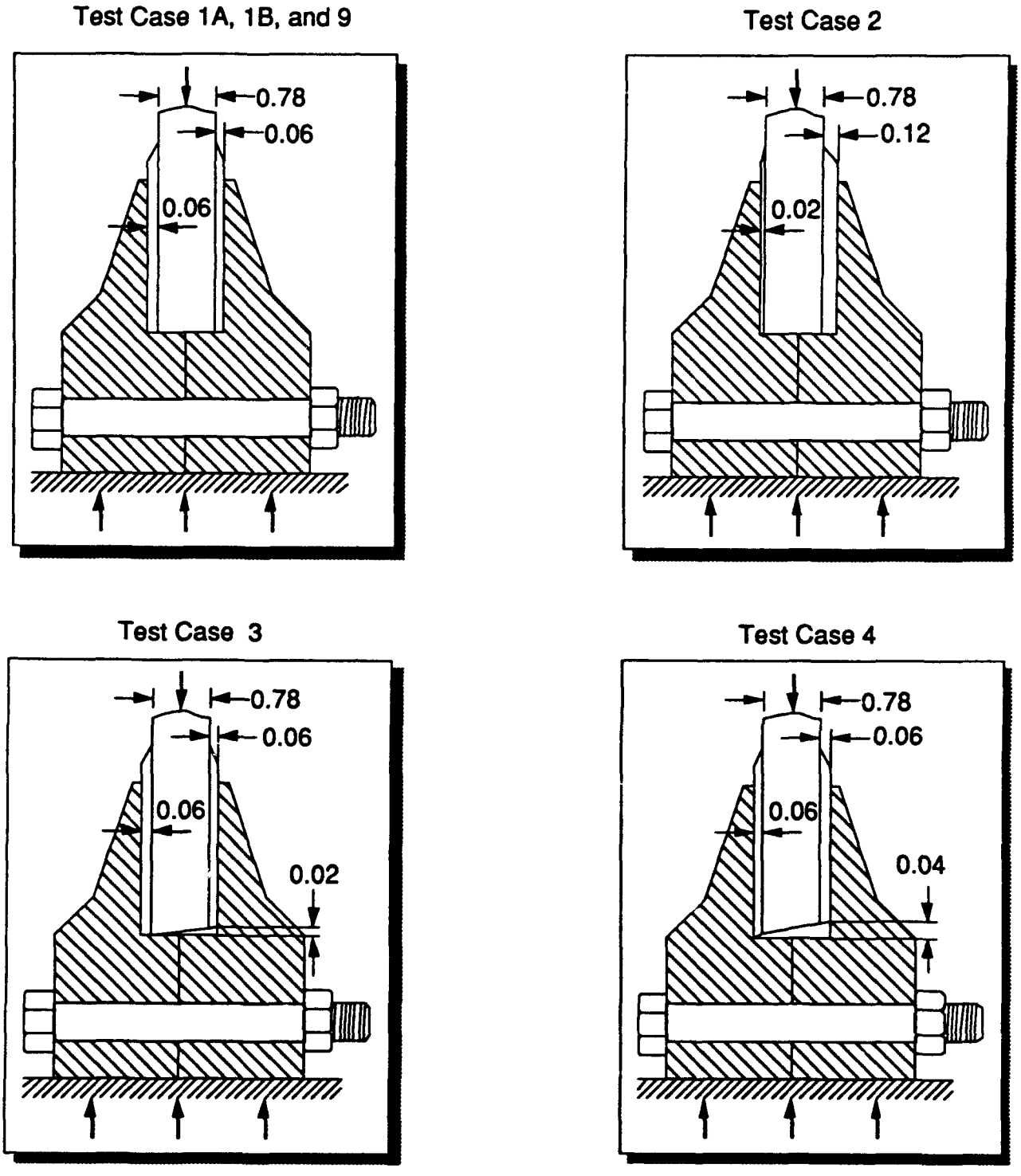


**Figure 4a. Schematic Representation of Each Test Case Geometry.**

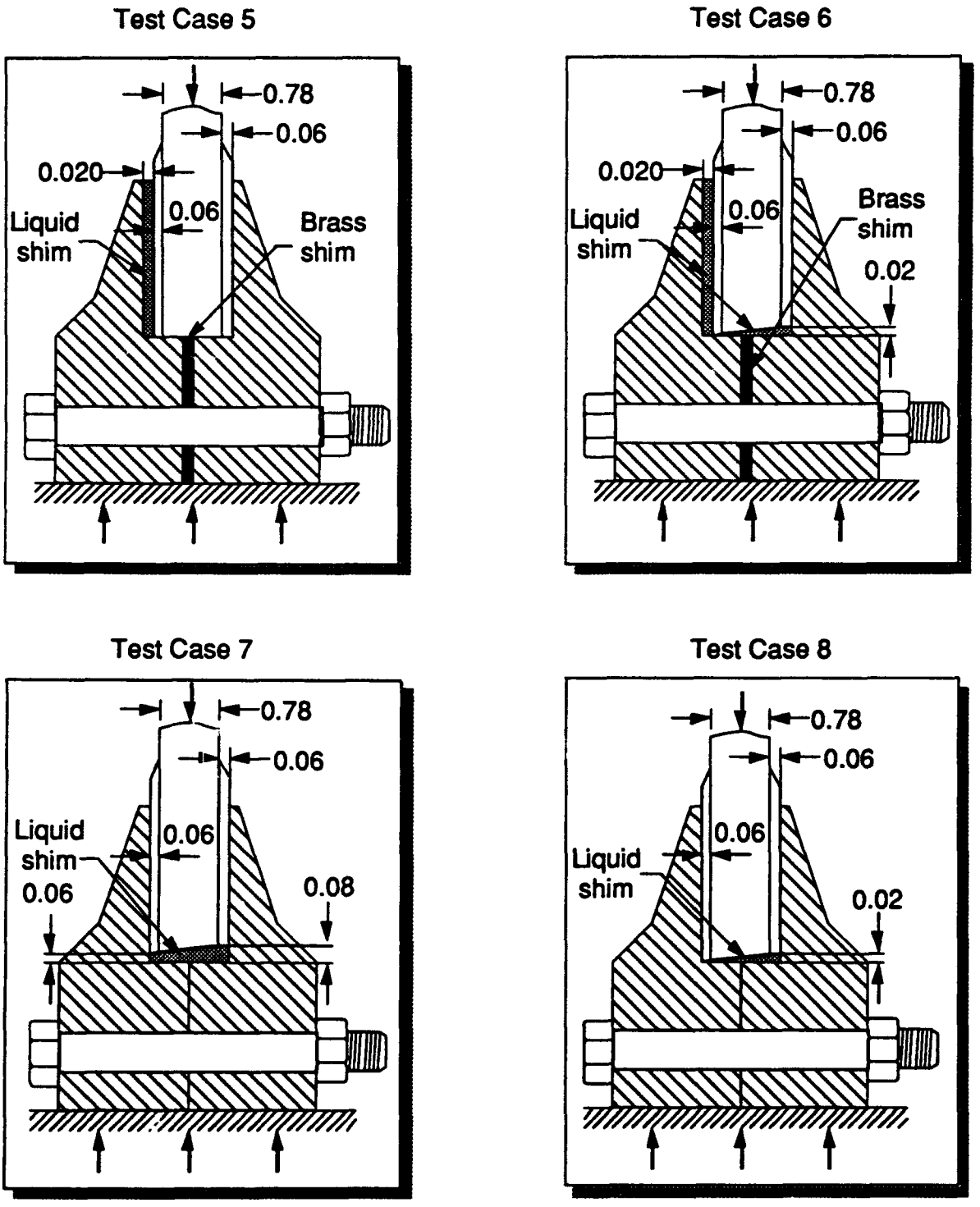


**Figure 4b. Schematic Representation of Each Test Case Geometry.**

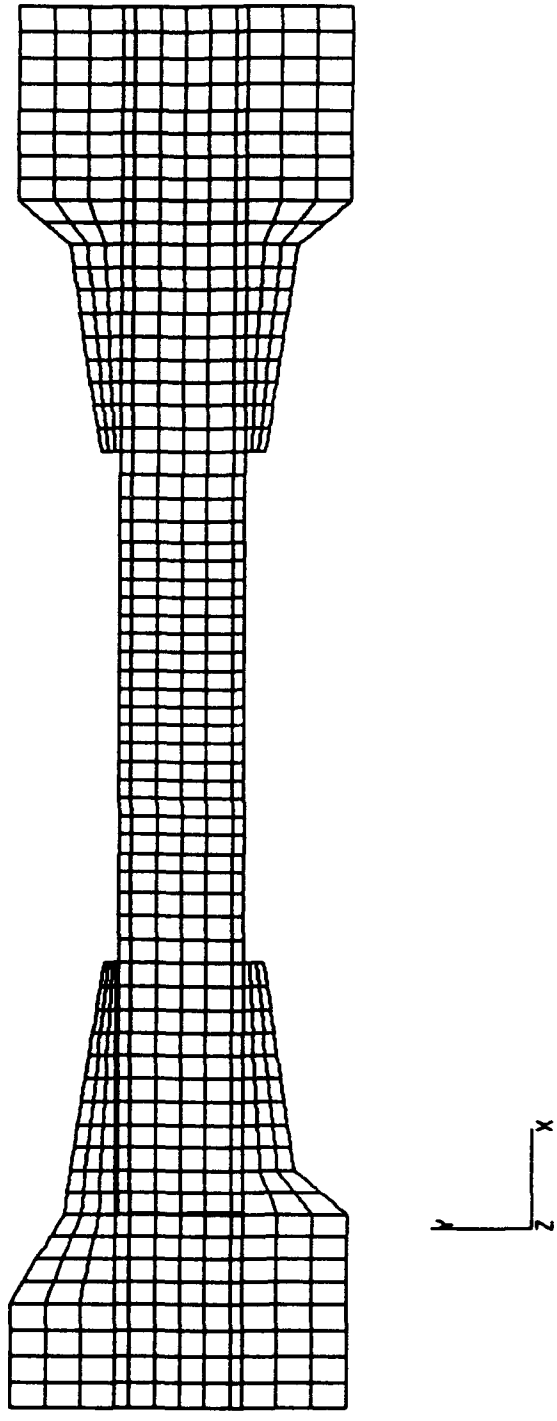


**Figure 5. Finite Element Model Mesh Used in the Analysis of the Sphere Joint Test Specimen.**

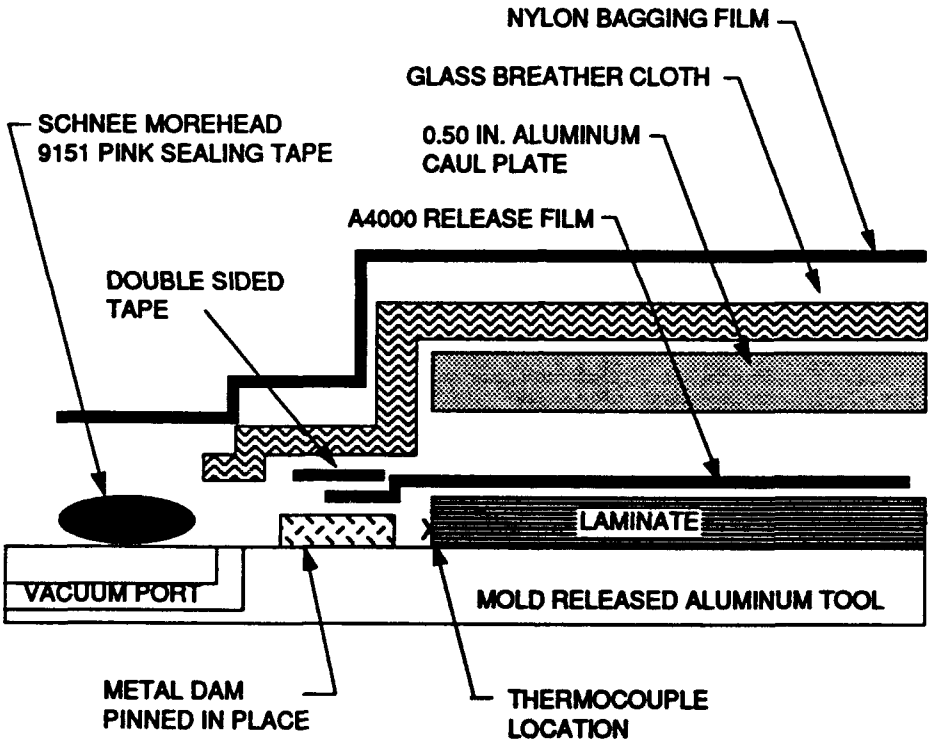


Figure 6. Schematic of the AS4/3501-6 Composite Panel Bagging Configuration.

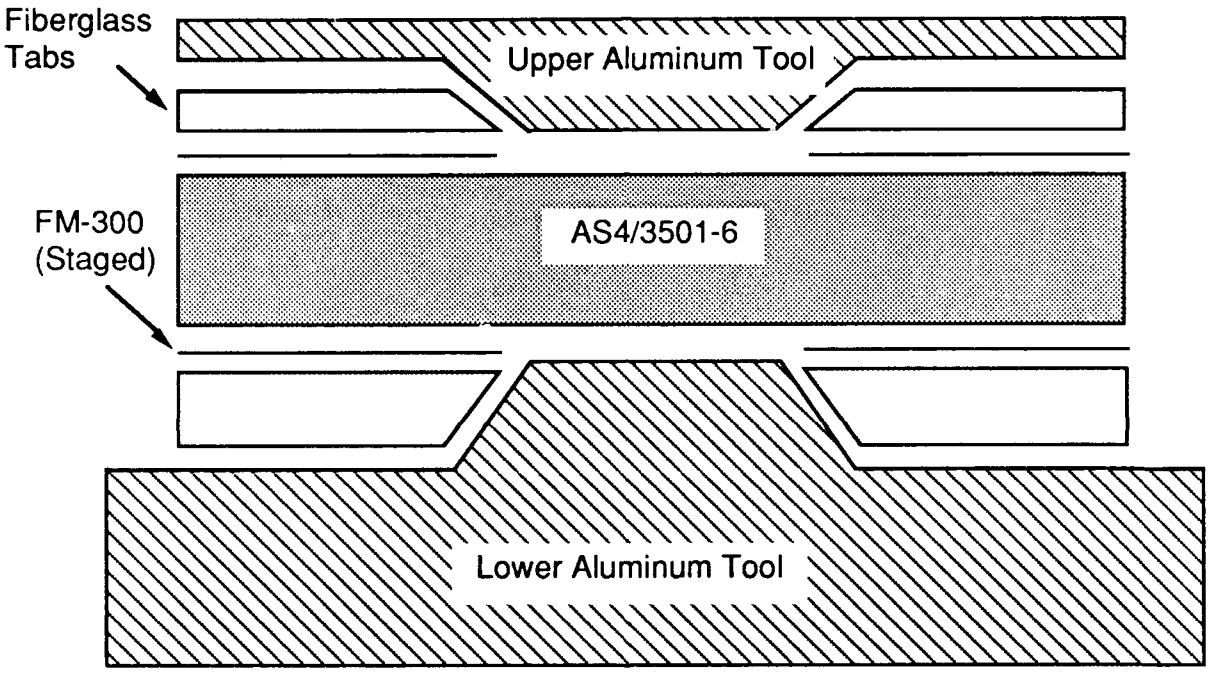


Figure 7. Tooling and Assembly Schematic for Cobonding Fiberglass End Tabs to Carbon/Epoxy Laminates.

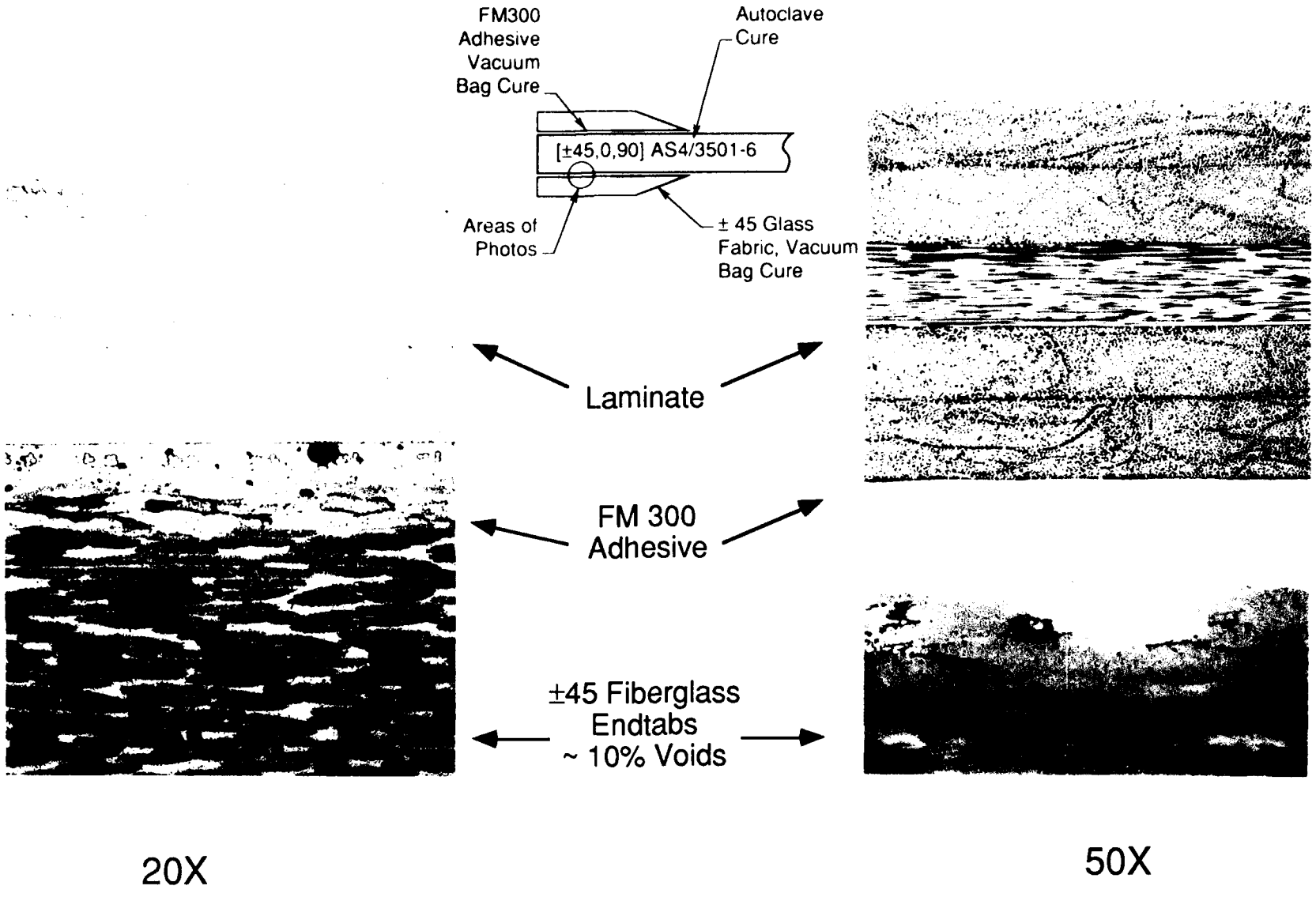


Figure 8. Photomicrograhs of Carbon/Epoxy Sphere Joint Test Specimen and Fiberglass/Epoxy Endtab Material.

## Compression Load Versus Strain for a Typical Glass/Epoxy End Tab

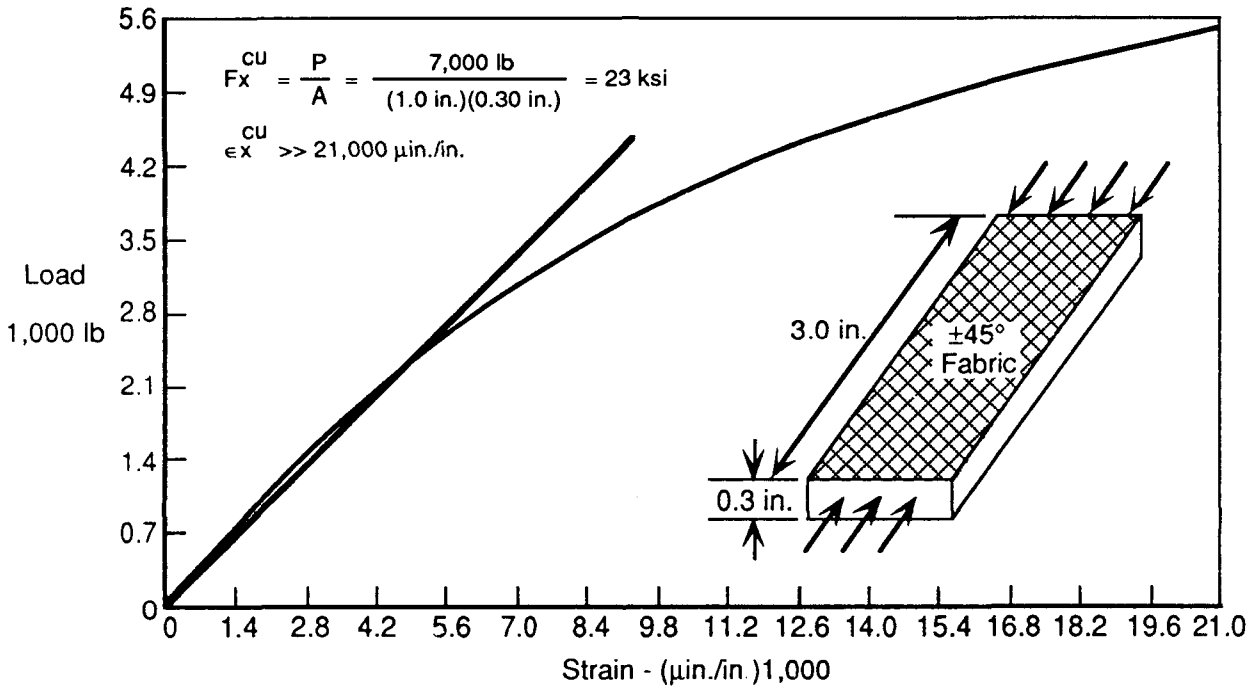


Figure 9. Compression Load vs Strain for a Typical [±45] Fiberglass/Epoxy End Tab.

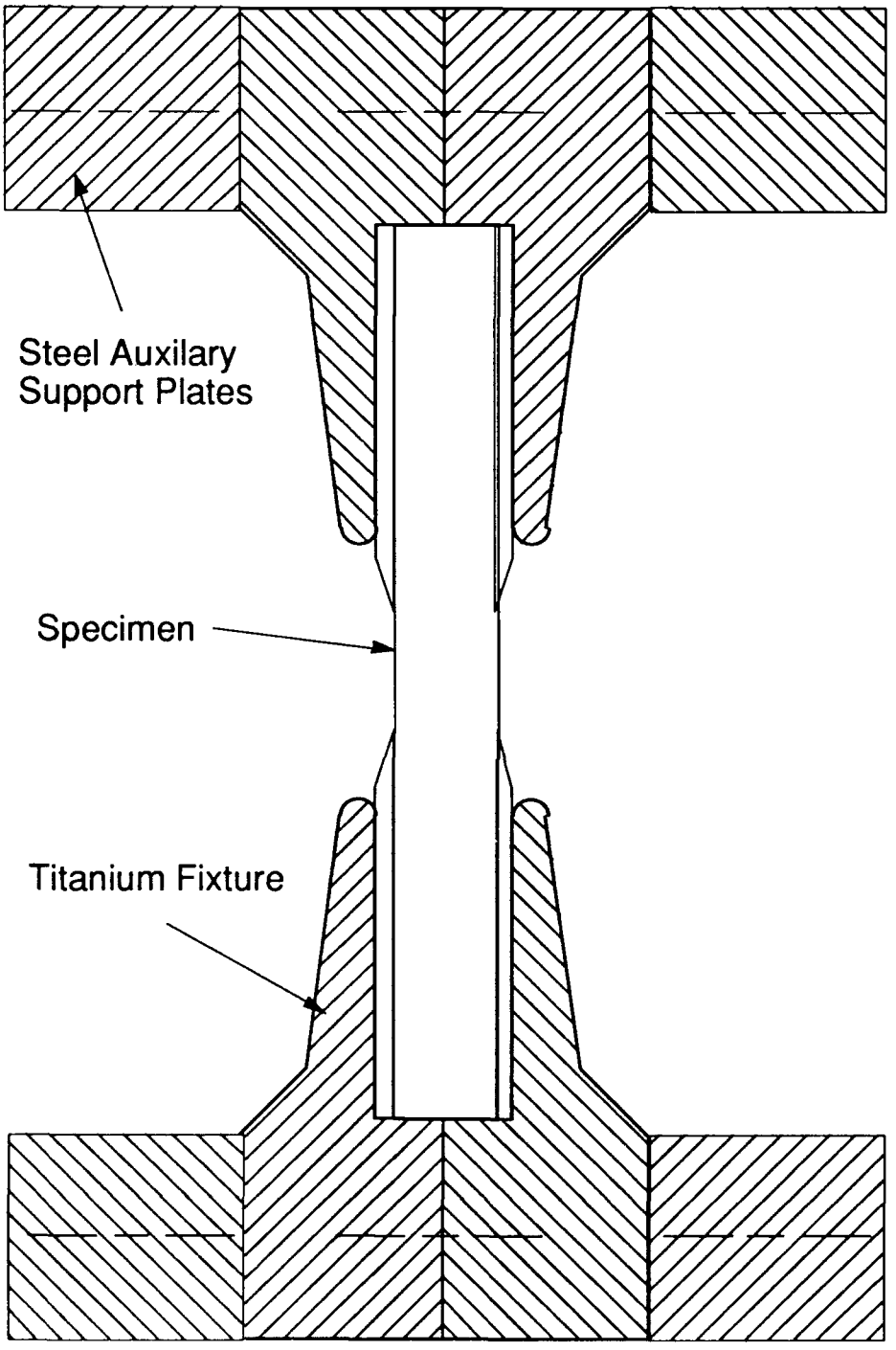


Figure 10. Schematic of Sphere Joint Test Fixture.

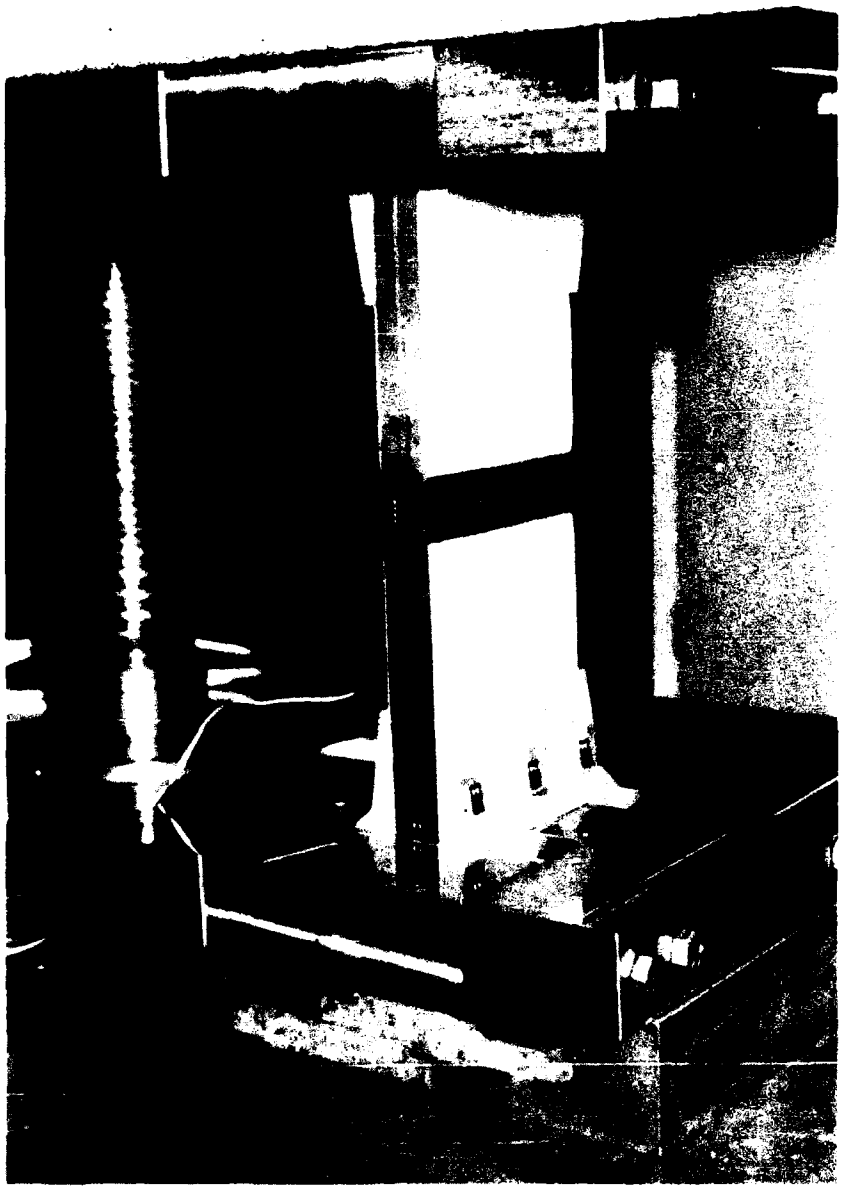

Figure 11. Photograph of Sphere Joint Test Fixture Assembly.

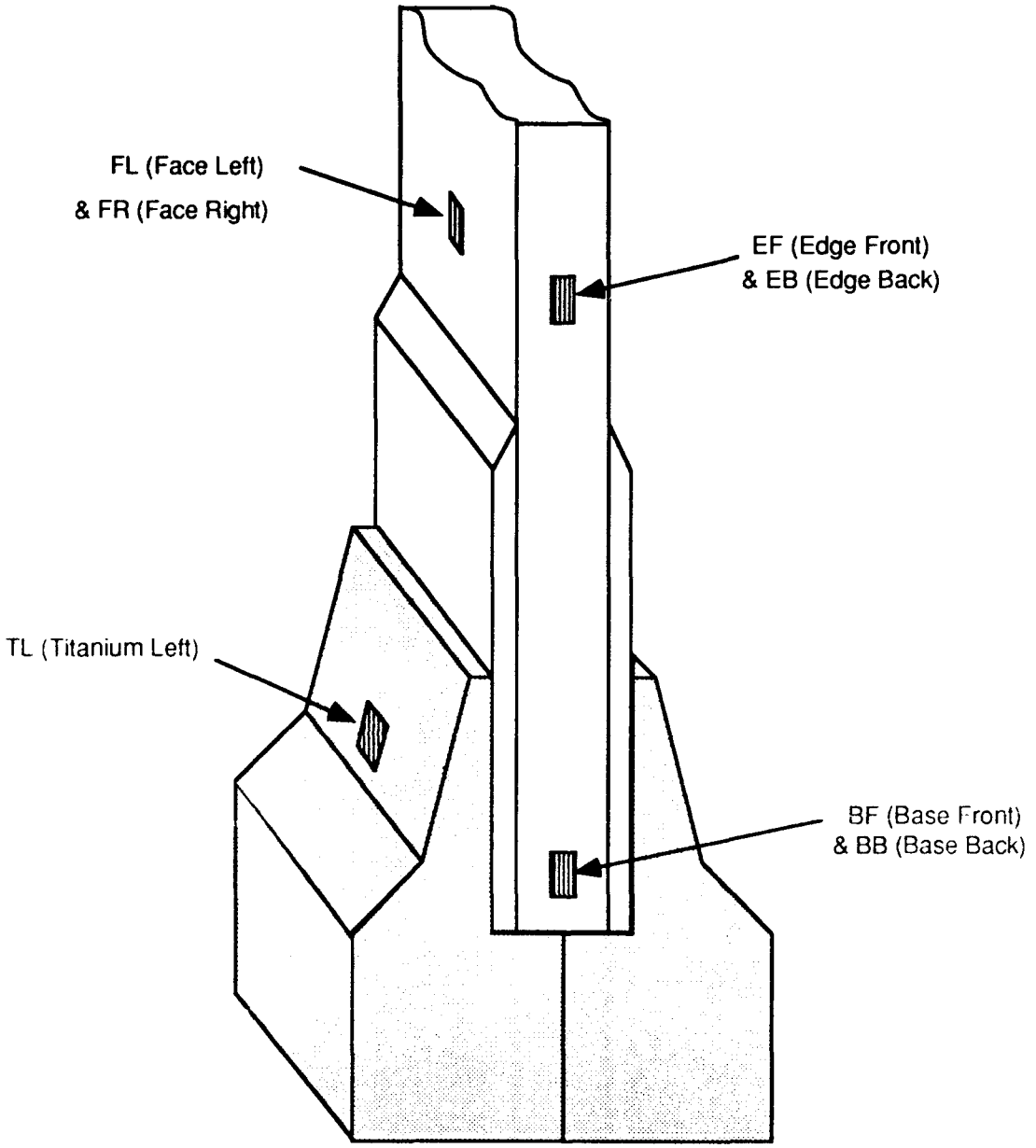


Figure 12. Strain Gage Location and Code for Square End Specimens.

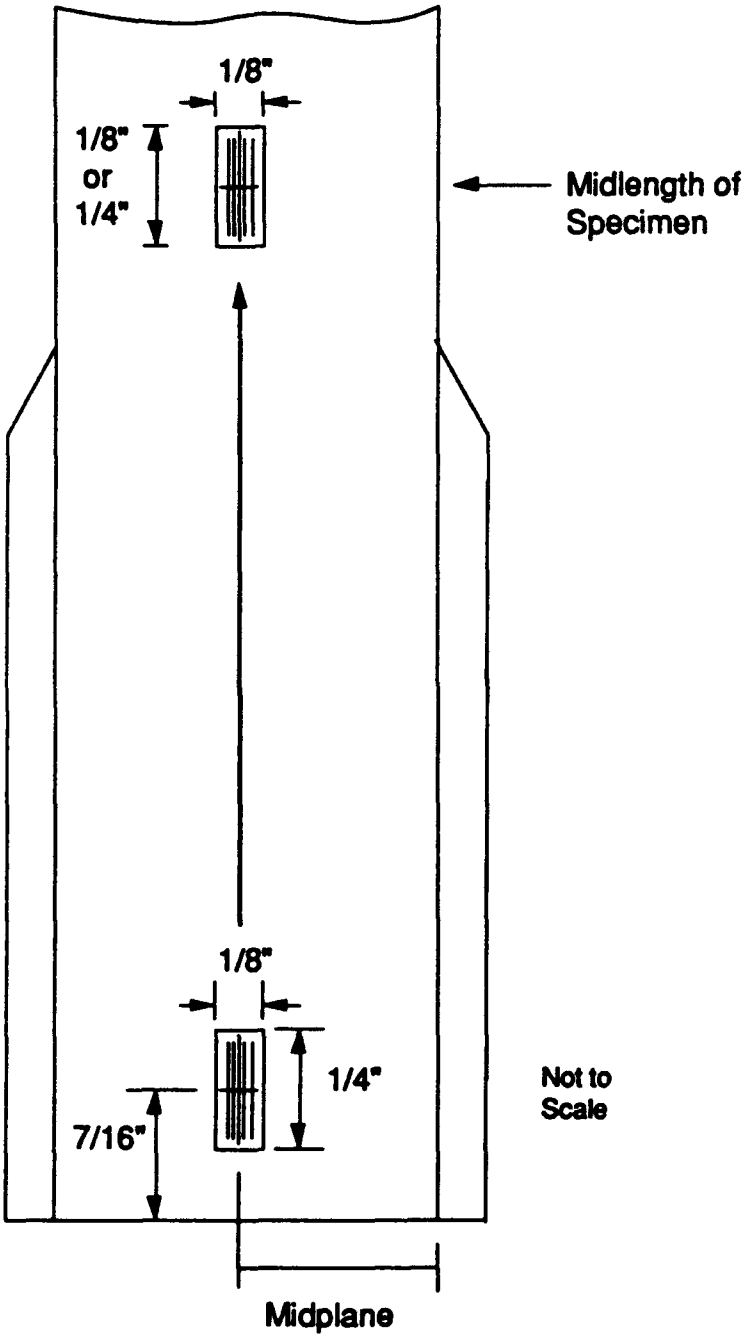


Figure 13. Strain Gage Dimensions for Square End Specimens.

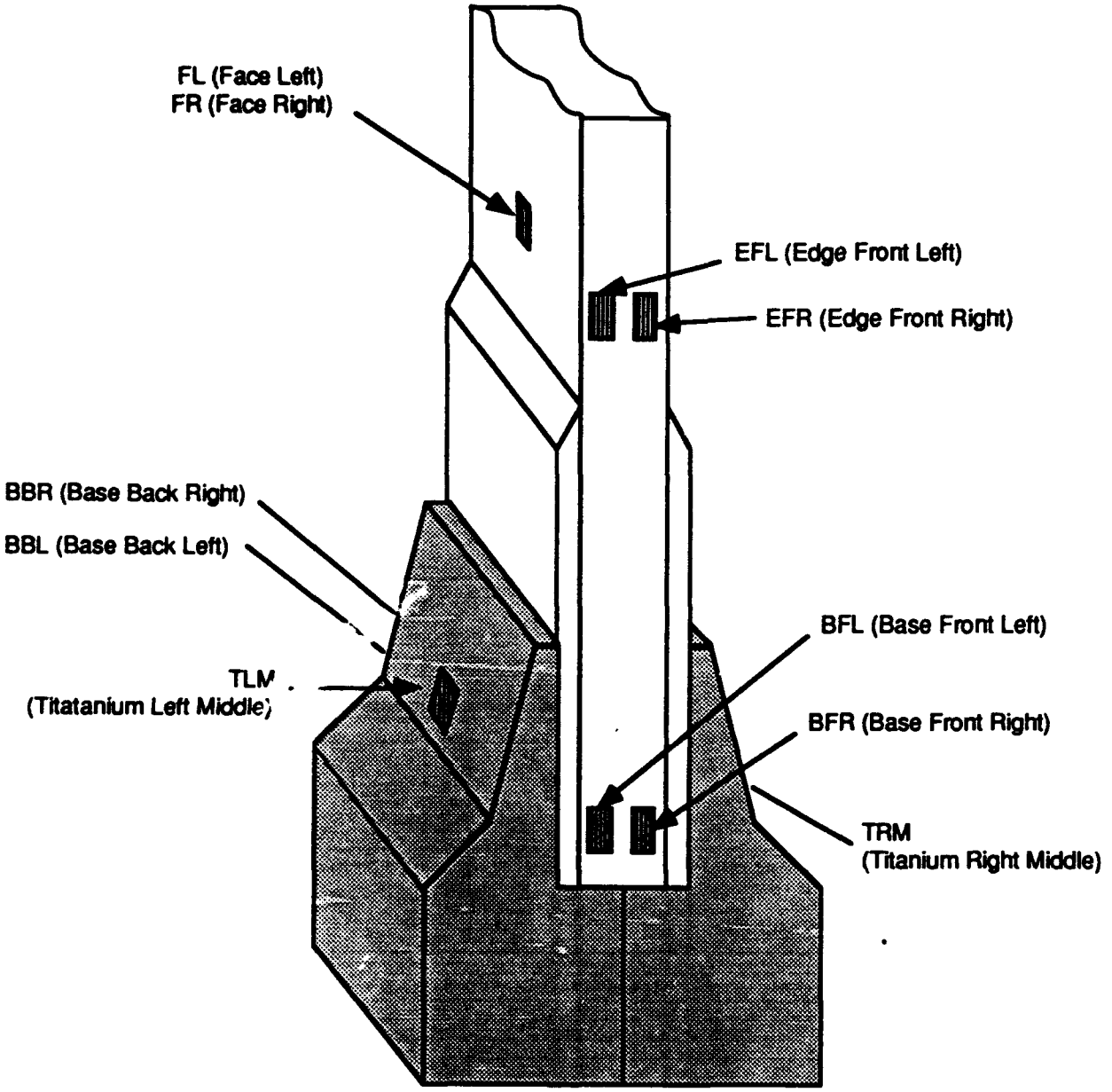


**Figure 14. Strain Gage Location and Code for Bevel End Specimens.**

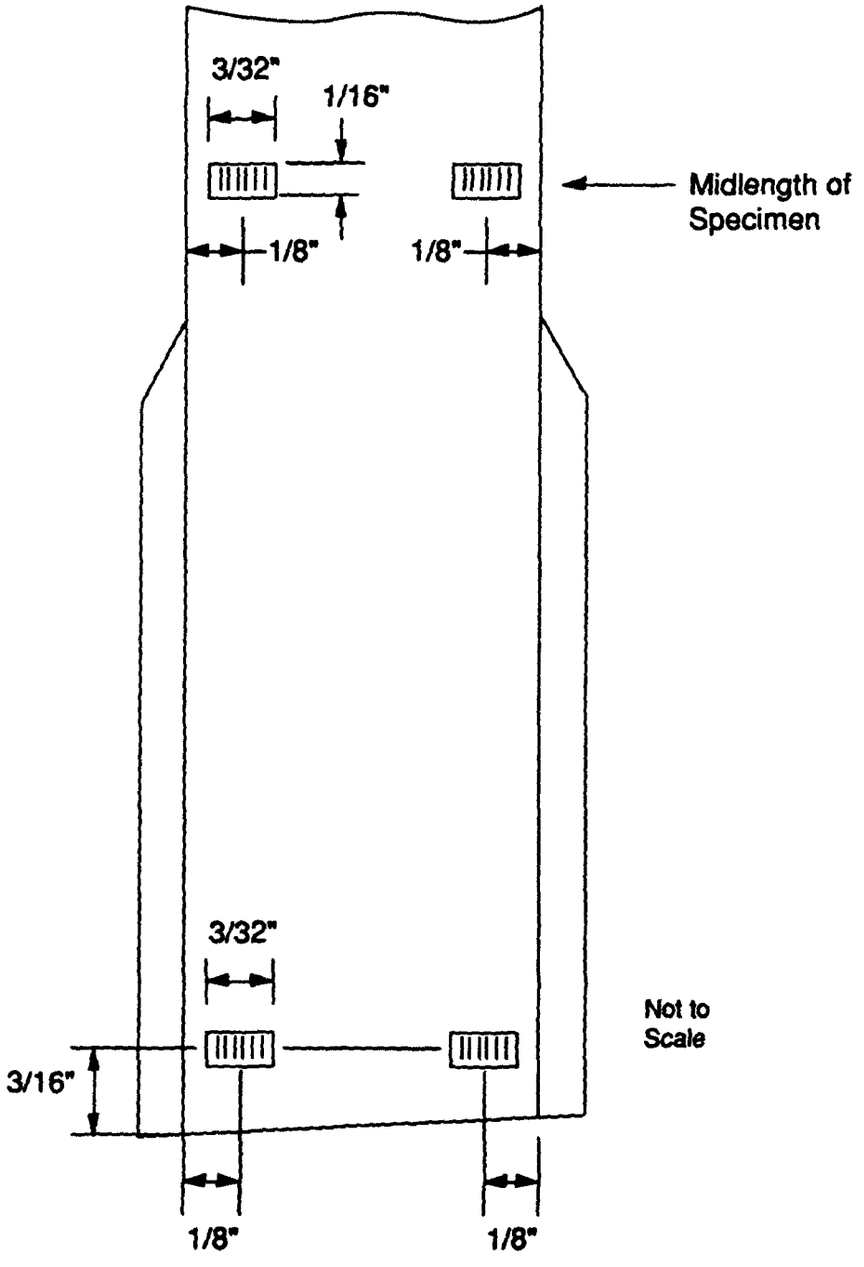


Figure 15. Strain Gage Dimensions for Bevel End Specimens.

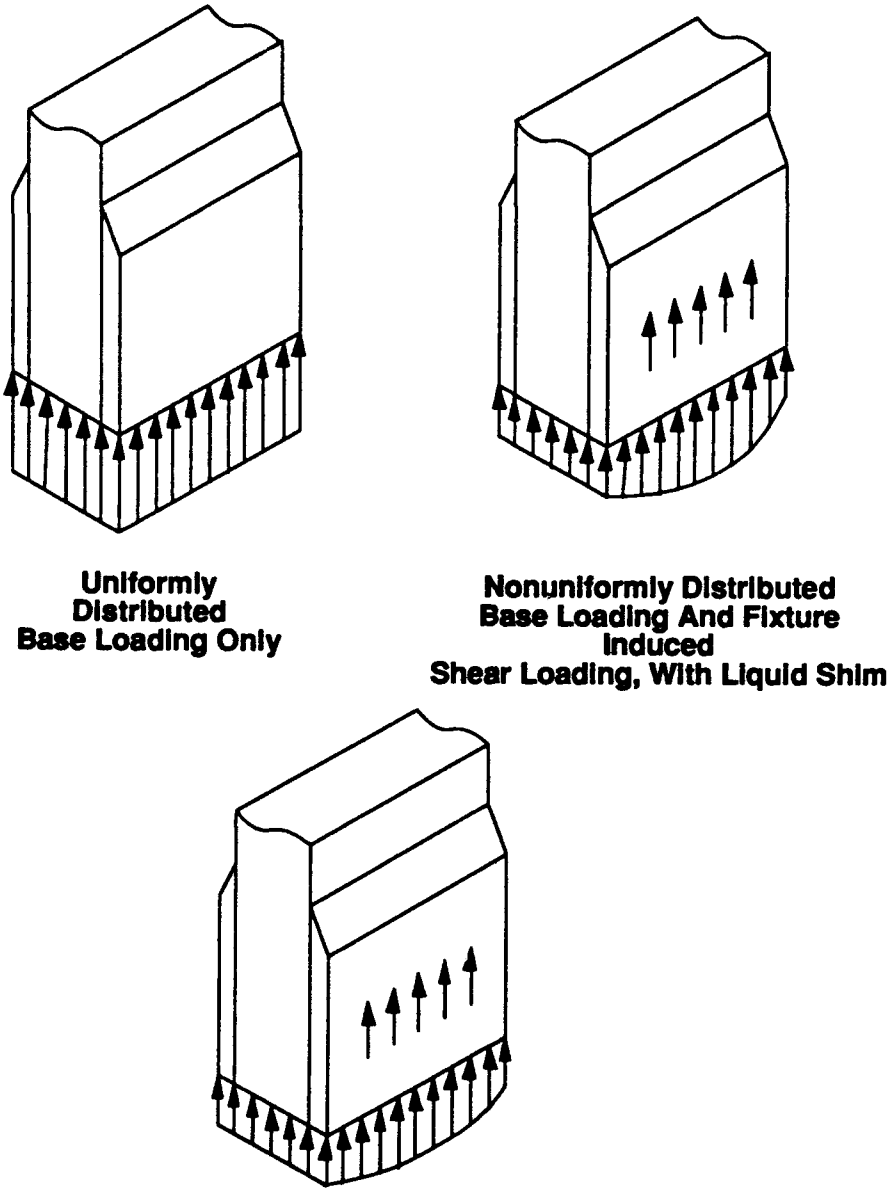


Figure 16. Schematic of Nonuniform Load Distribution at Specimen Base.

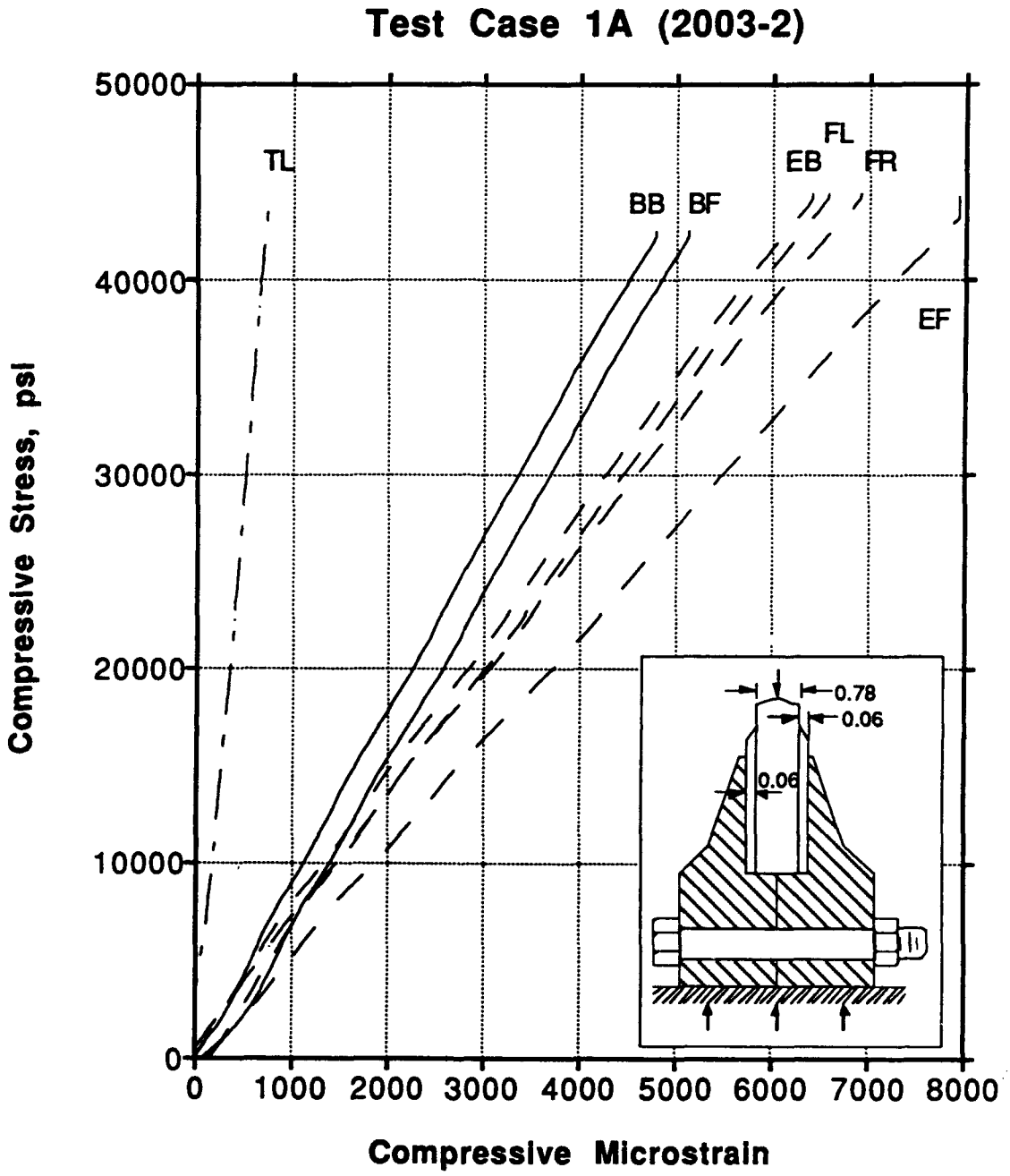


Figure 17 Compression Stress-Strain Curve for Test Case 1A, Spec. 2003-2.

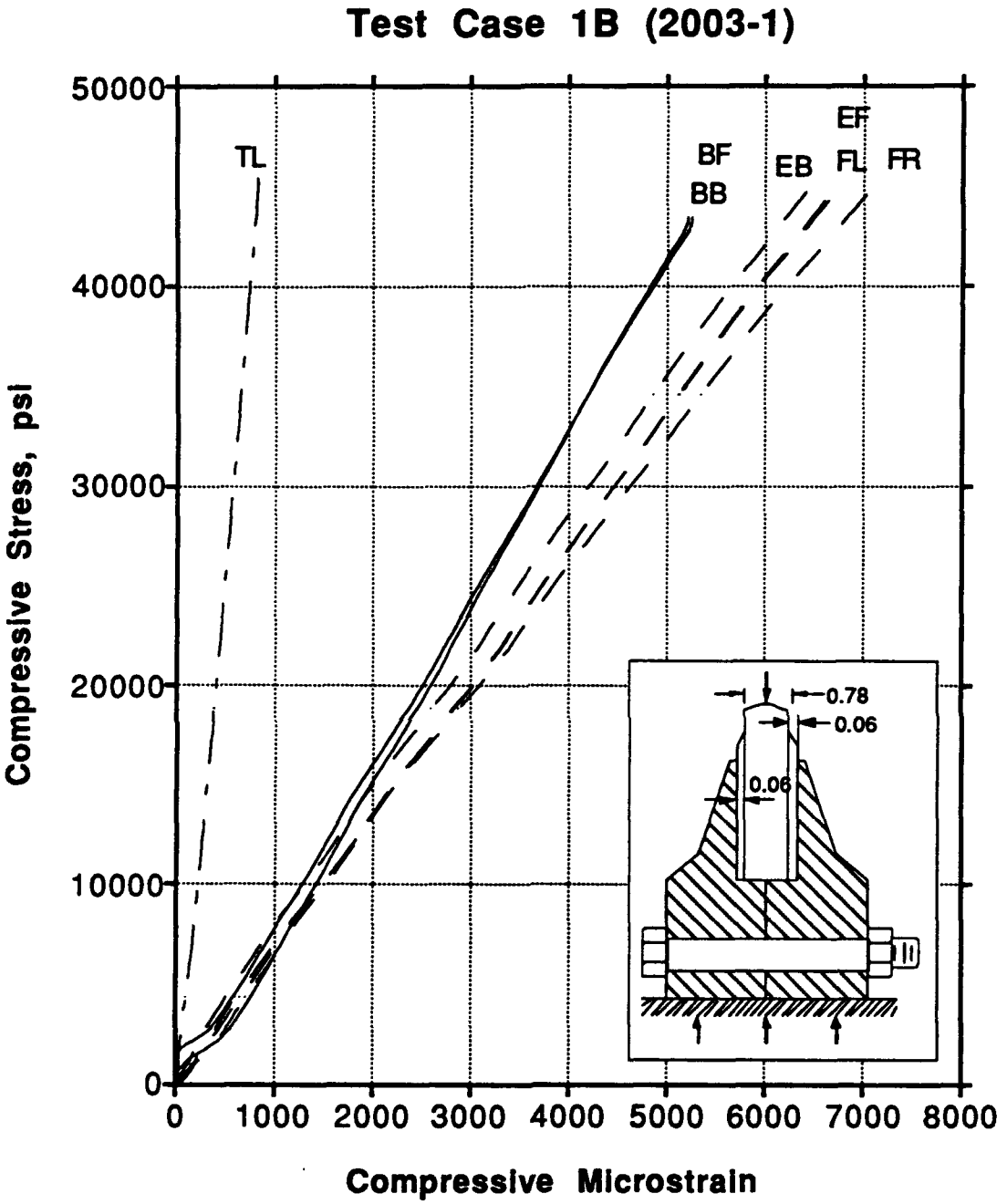


Figure 18 Compression Stress-Strain Curve for Test Case 1A, Spec. 2003-2.

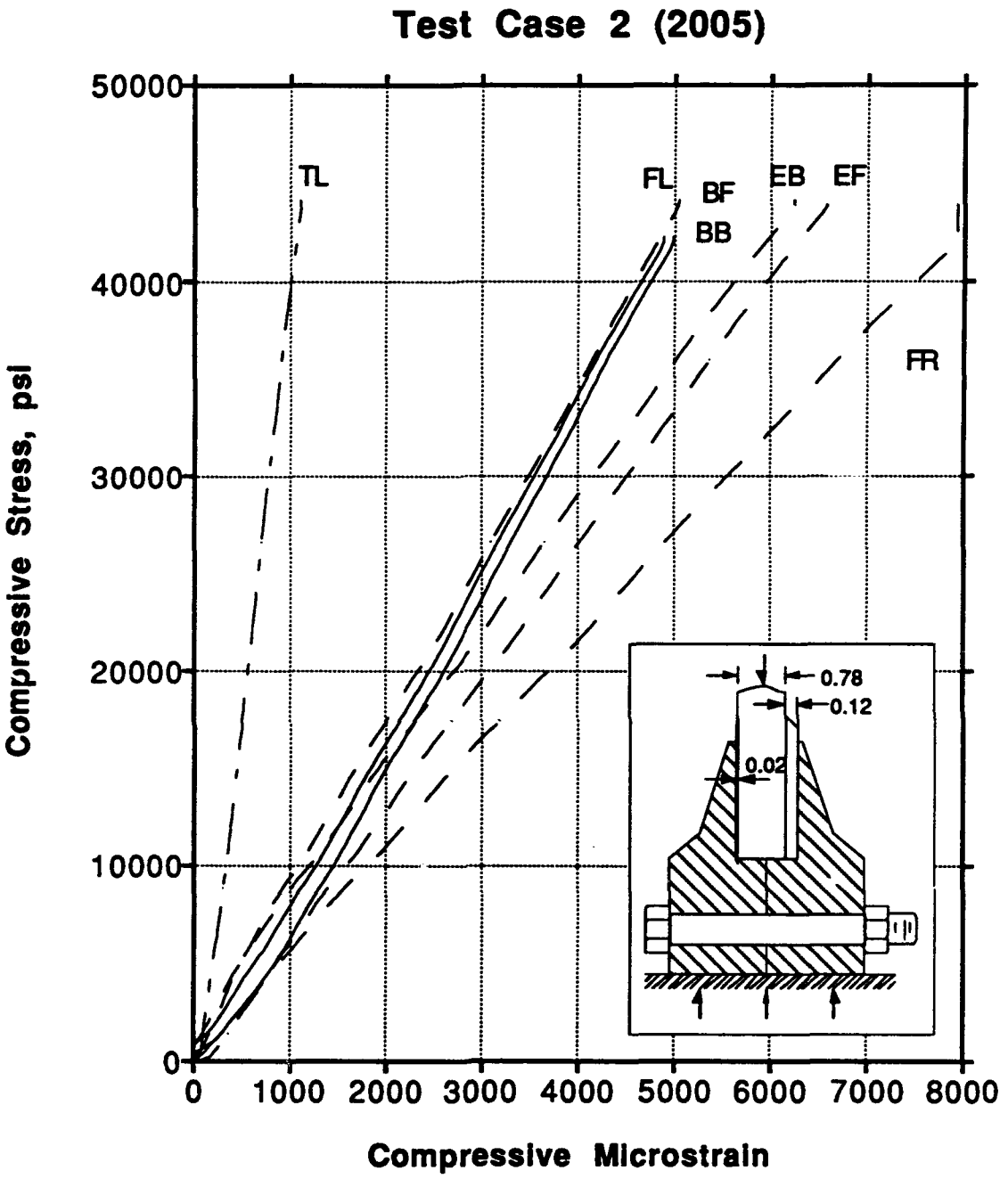


Figure 19 Compression Stress-Strain Curve for Test Case 2, Spec. 2005.

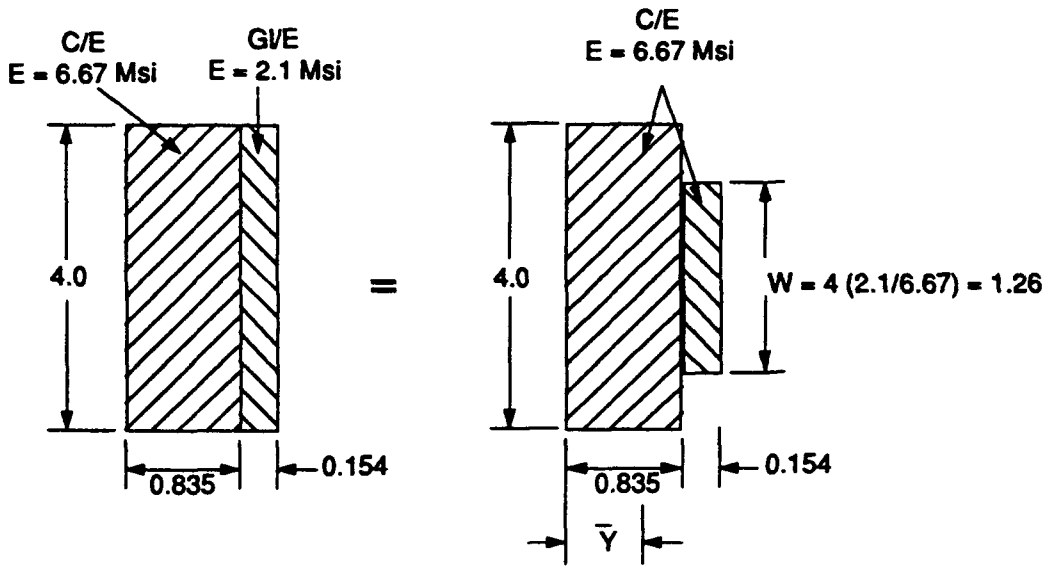


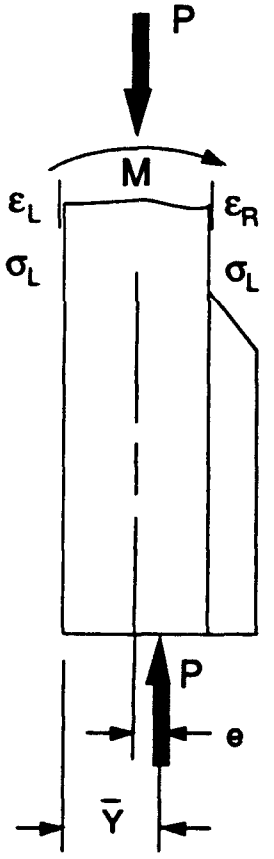


$$\bar{Y} = \frac{\Sigma AY}{\Sigma A} = \frac{(0.835)(4)(0.835/2) + (0.154)(1.26)(0.835 + 0.154/2)}{(0.835)(4) + (0.154)(1.26)}$$

$\bar{Y} = 0.444$ in.

$e = \bar{Y} - (0.835/2) = 0.444 - 0.417 = 0.027$

$M = (P)(e) = (\sigma)(A)(e) = (44{,}000 \text{ psi})(0.835 \text{ in})(4 \text{ in})(0.027 \text{ in})$

$M = 3{,}968$ in-lbs

$$\sigma = \frac{P}{(w)(t)} \pm \frac{6M}{(w)(t)^2}$$

$$\sigma_L = \frac{-146{,}960}{(4)(0.835)} + \frac{6(3{,}968)}{(4)(0.835)^2} = -35{,}460 \text{ psi}$$

$$\sigma_R = \frac{-146{,}960}{(4)(0.835)} - \frac{6(3{,}968)}{(4)(0.835)^2} = -52{,}540 \text{ psi}$$

$$\varepsilon_L = \frac{-35{,}460 \text{ psi}}{6.67 \text{ Msi}} = -5{,}316 \ \mu\frac{\text{in}}{\text{in}}$$

$$\varepsilon_R = \frac{-52{,}540 \text{ psi}}{6.67 \text{ Msi}} = -7{,}877 \ \mu\frac{\text{in}}{\text{in}}$$

Figure 20 Free-Body Diagram of Load Eccentricity Due to Unequal tab Thickness.

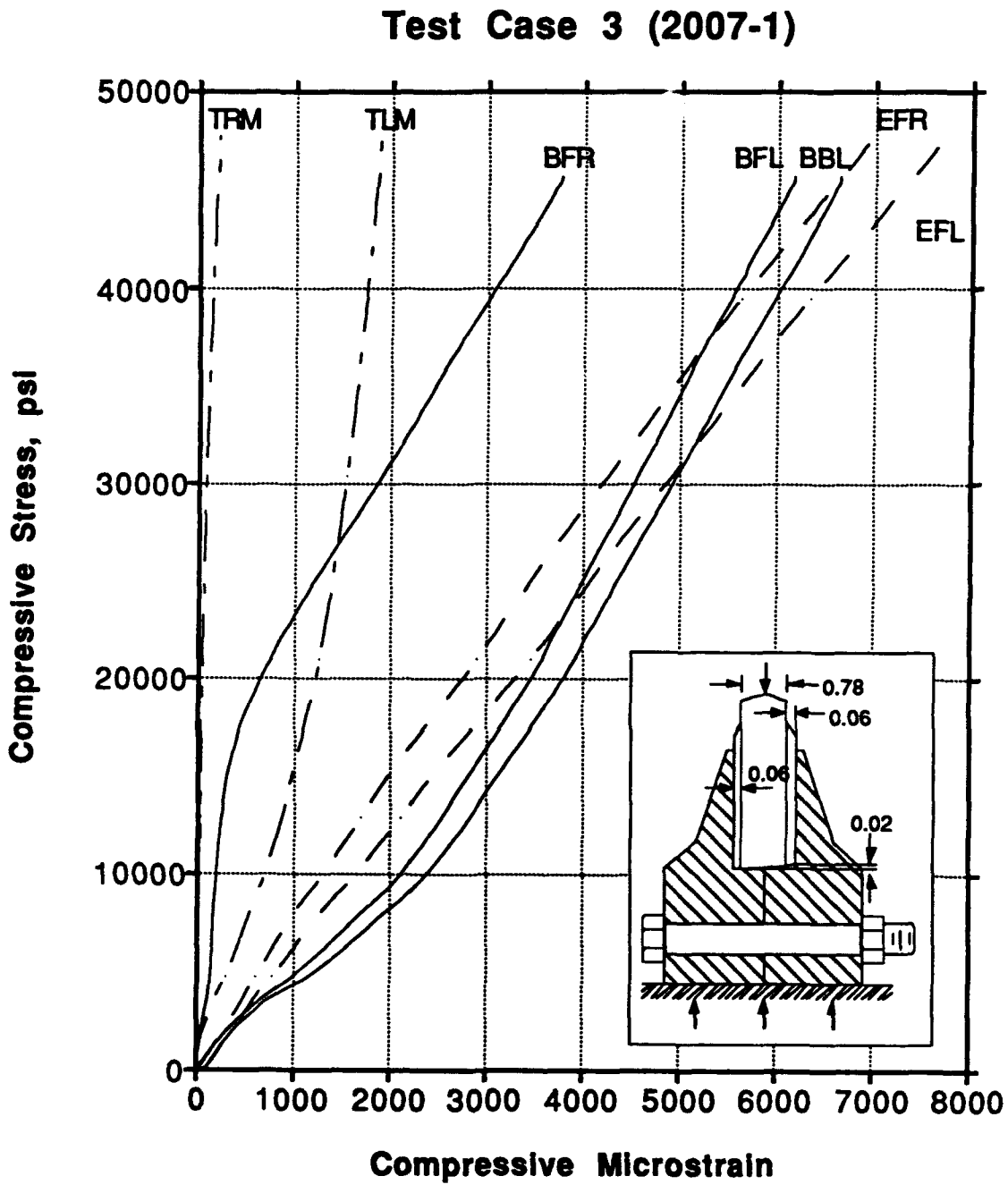


Figure 21 Compression Stress-Strain Curve for Test Case 3, Spec. 2007-1.

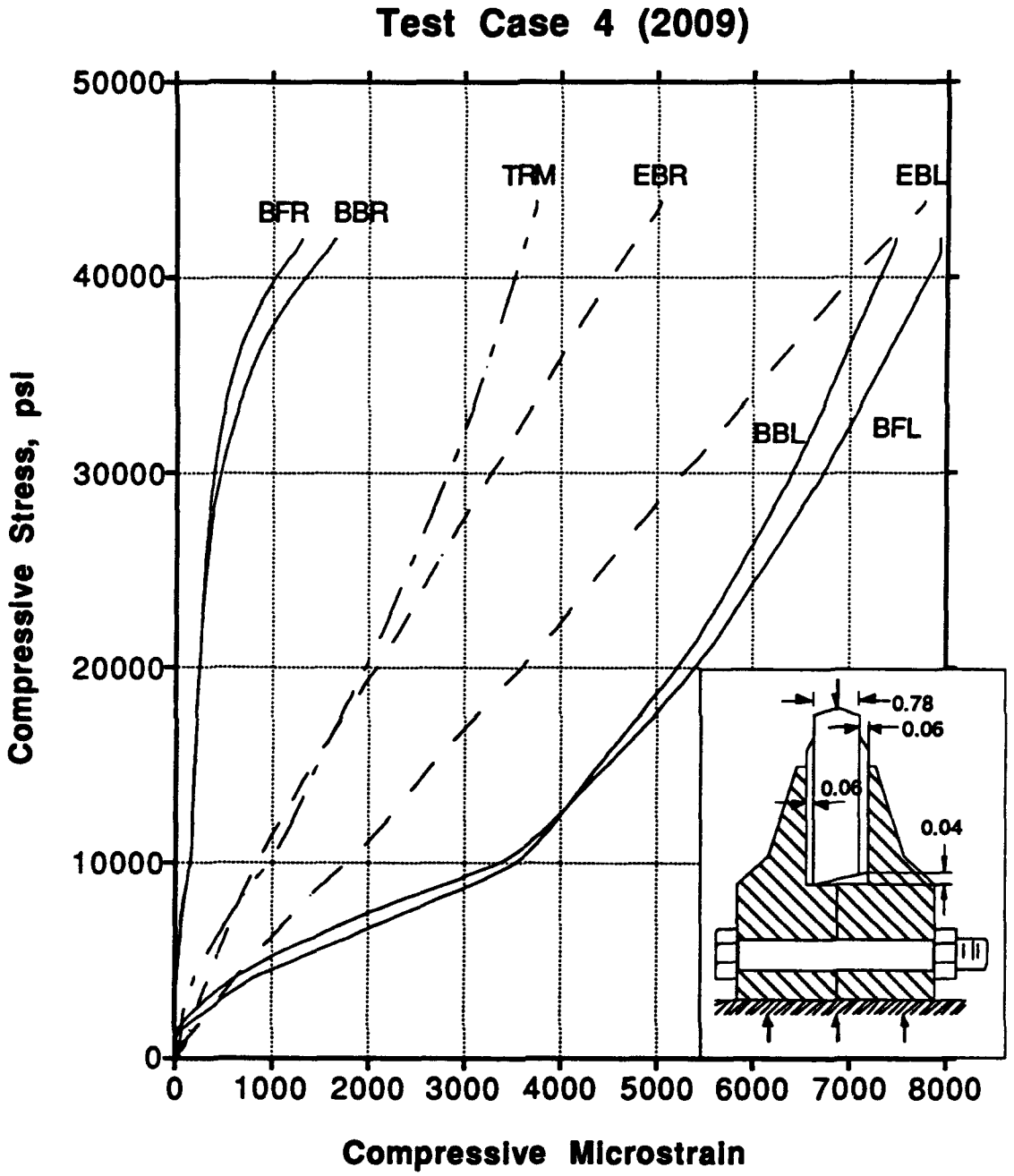


Figure 22 Compression Stress-Strain Curve for Test Case 4, Spec. 2009.

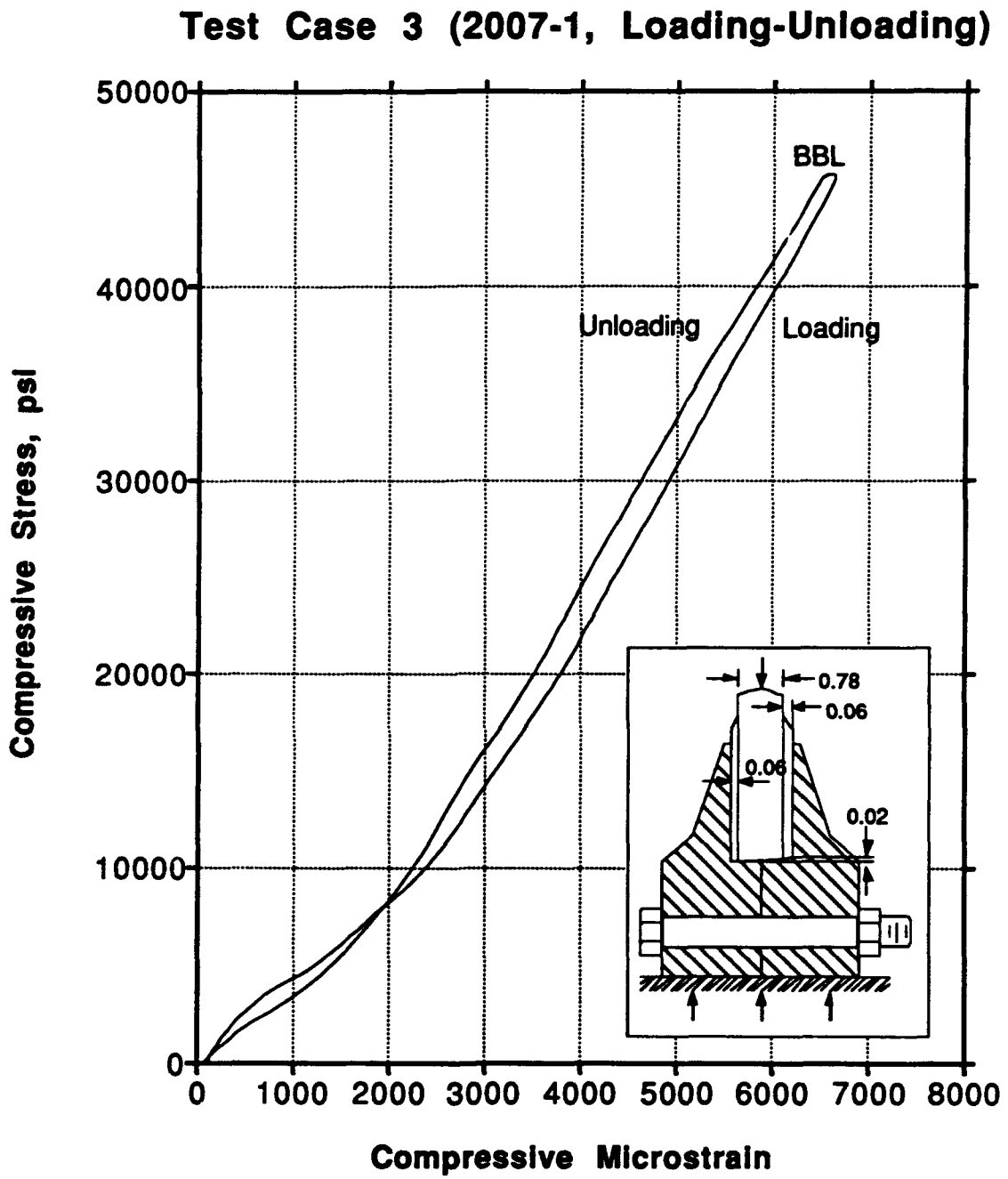


Figure 23 Unloading Stress-Strain Curve for Test Case 3, Spec. 2007-1.

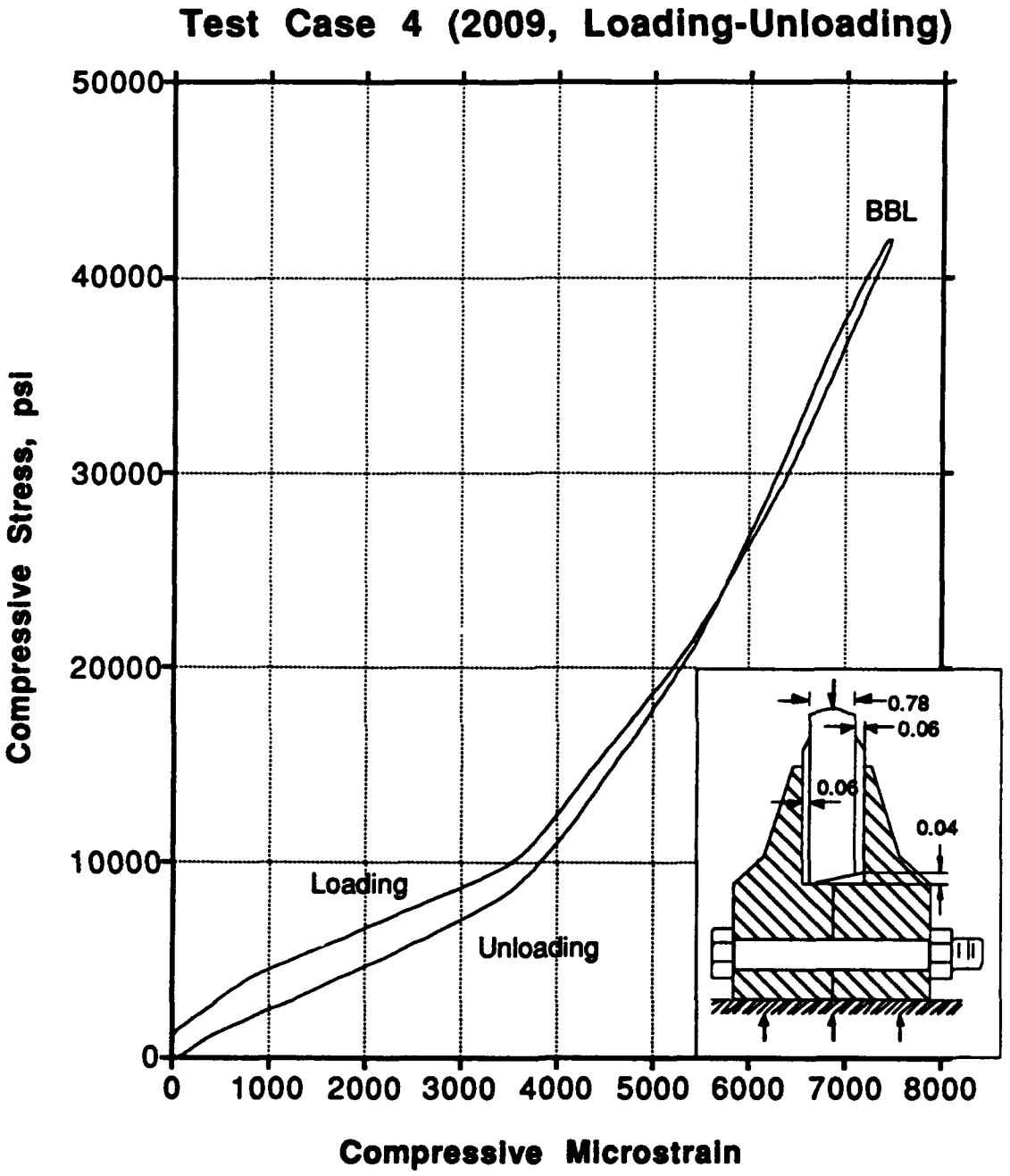


Figure 24 Unloading Stress-Strain Curve for Test Case 4, Spec. 2009.

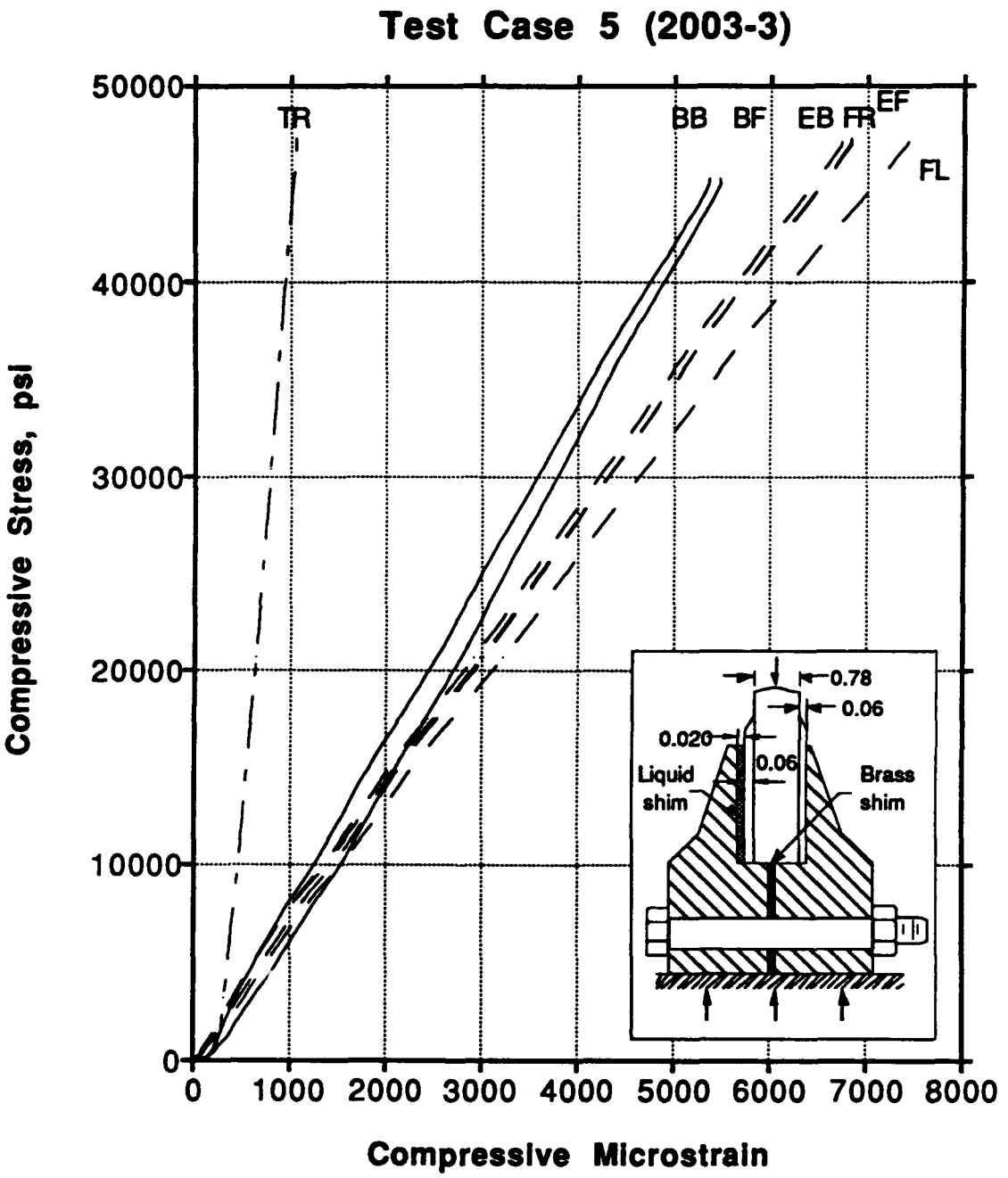


Figure 25 Compression Stress-Strain Curve for Test Case 5, Spec. 2003-3.

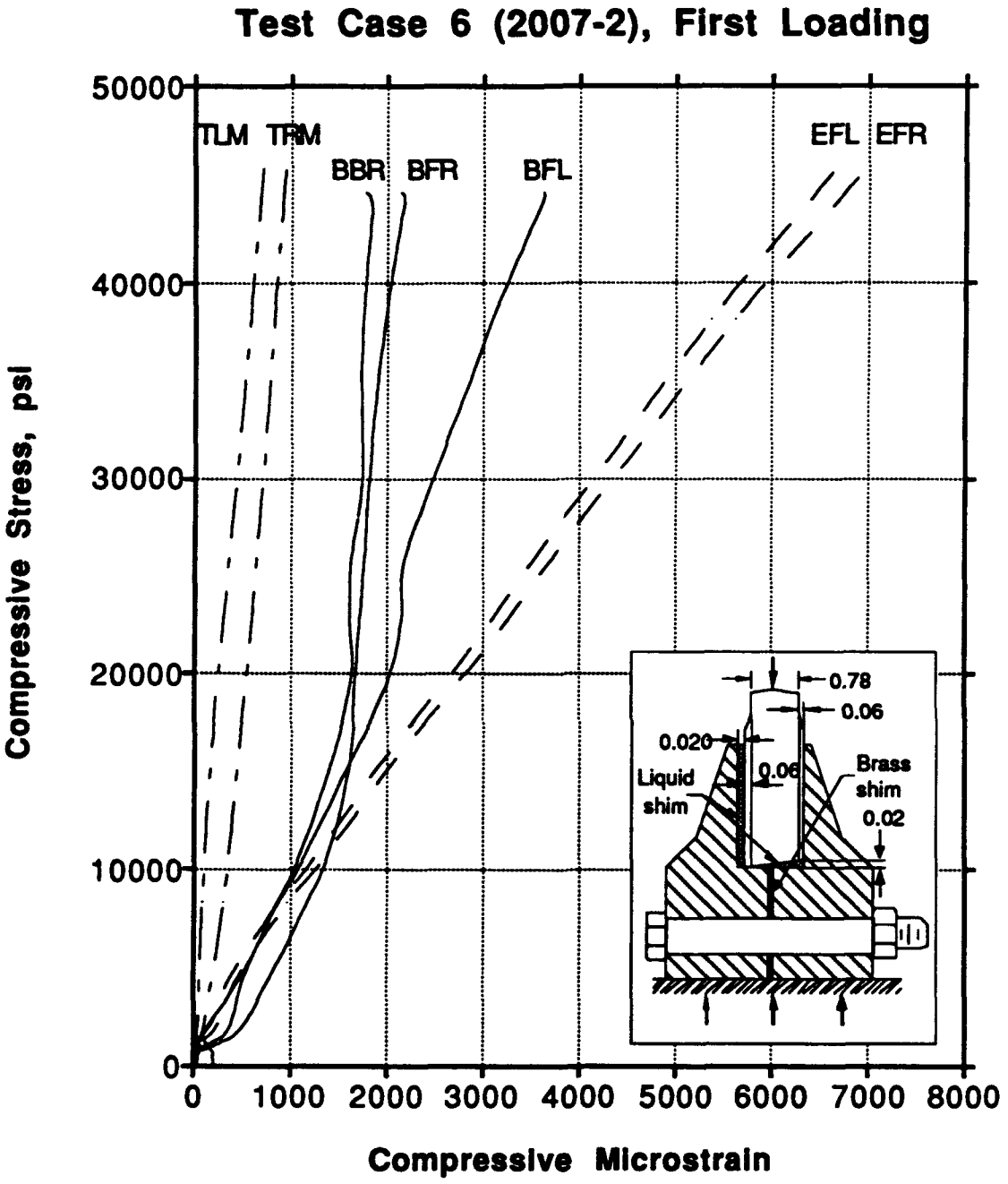


Figure 26 Compression Stress-Strain Curve for Test Case 6, 1st Loading, Spec. 2007-2.

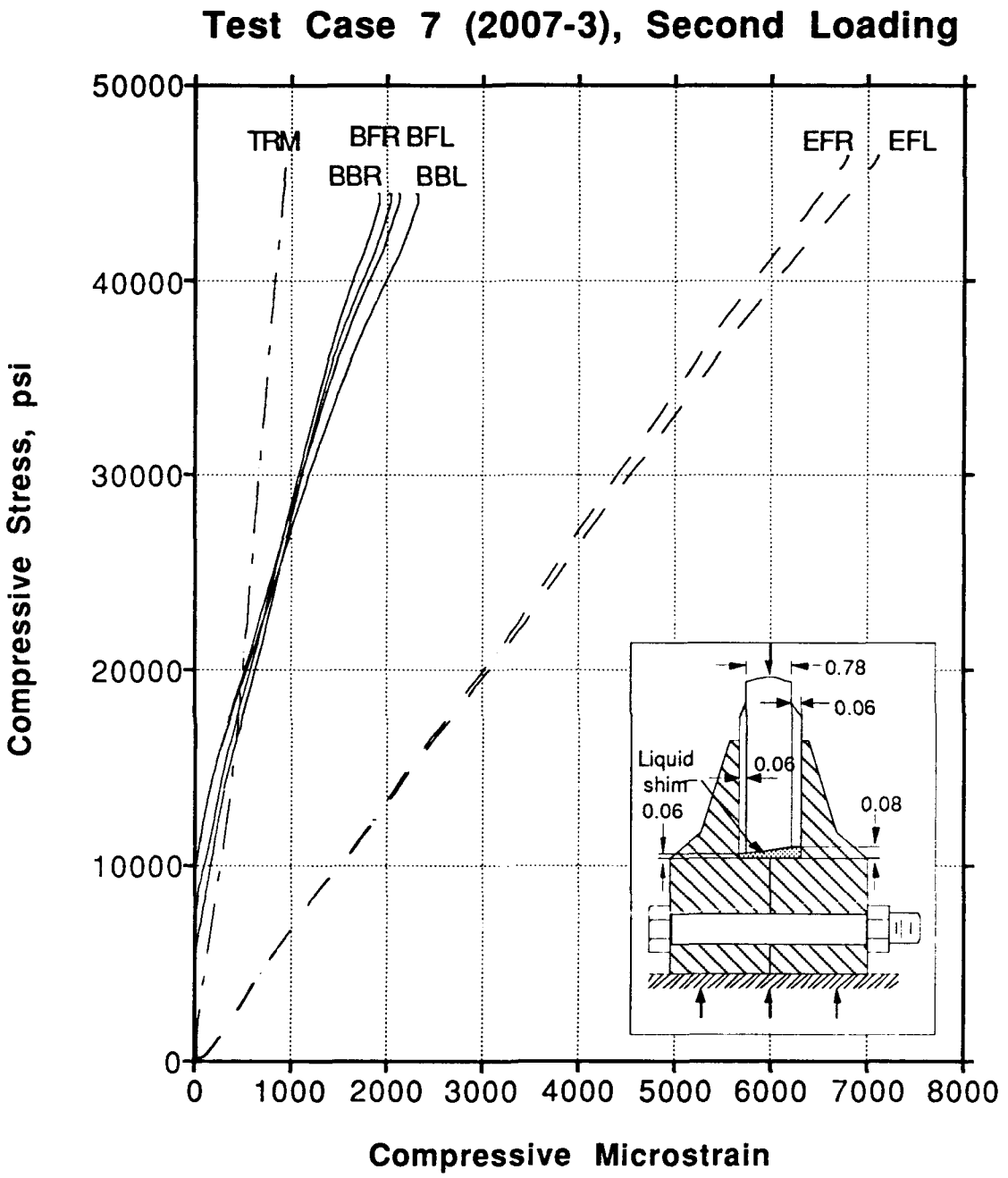


Figure 29 Compression Stress-Strain Curve for Test Case 7, 2nd Loading, Spec. 2007-3.

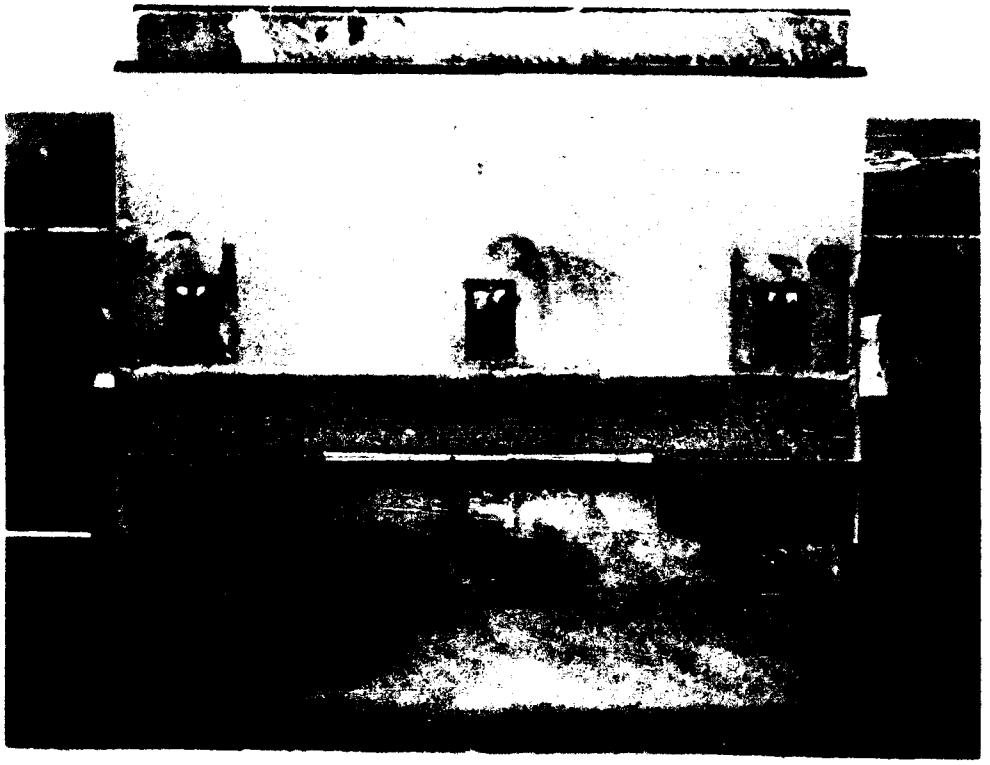

Figure 30 Photograph Showing Plastic Flow of Liquid Shim.

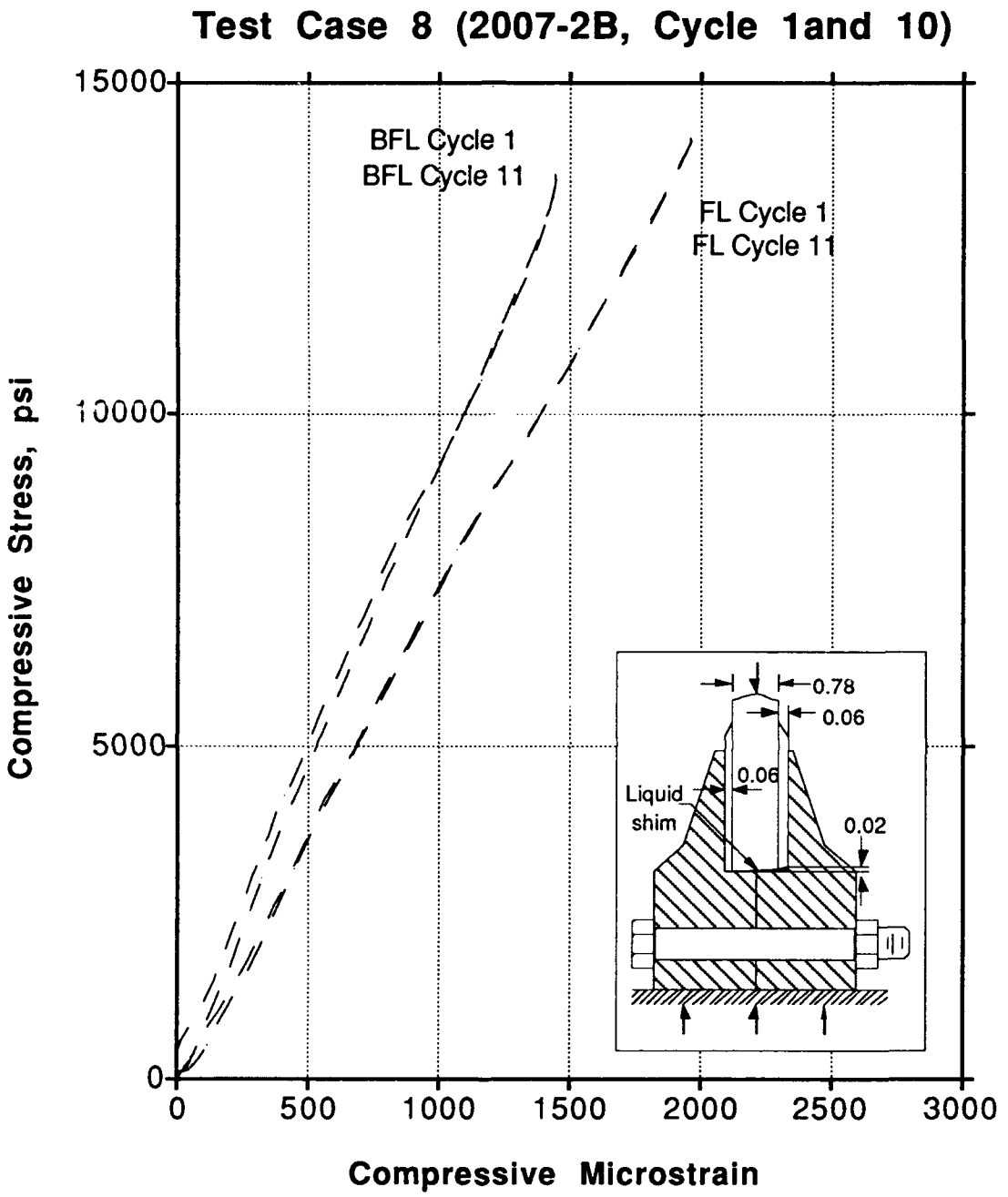


Figure 31 Compression Stress-Strain Curve for Cycle 1 and 10 of Test Case 8.

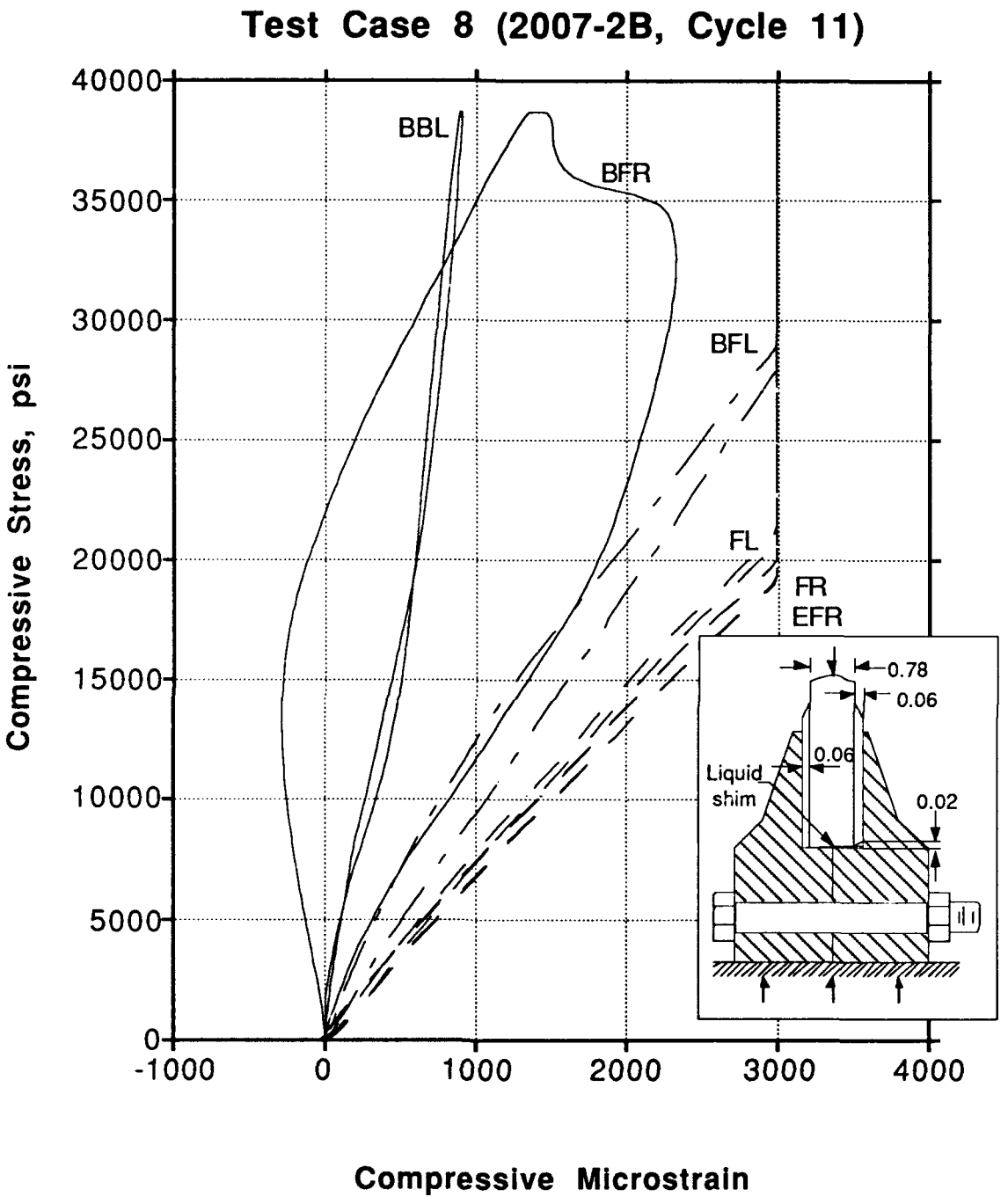


Figure 32 Compression Stress-Strain Curve for Cycle 11 of Test Case 8.

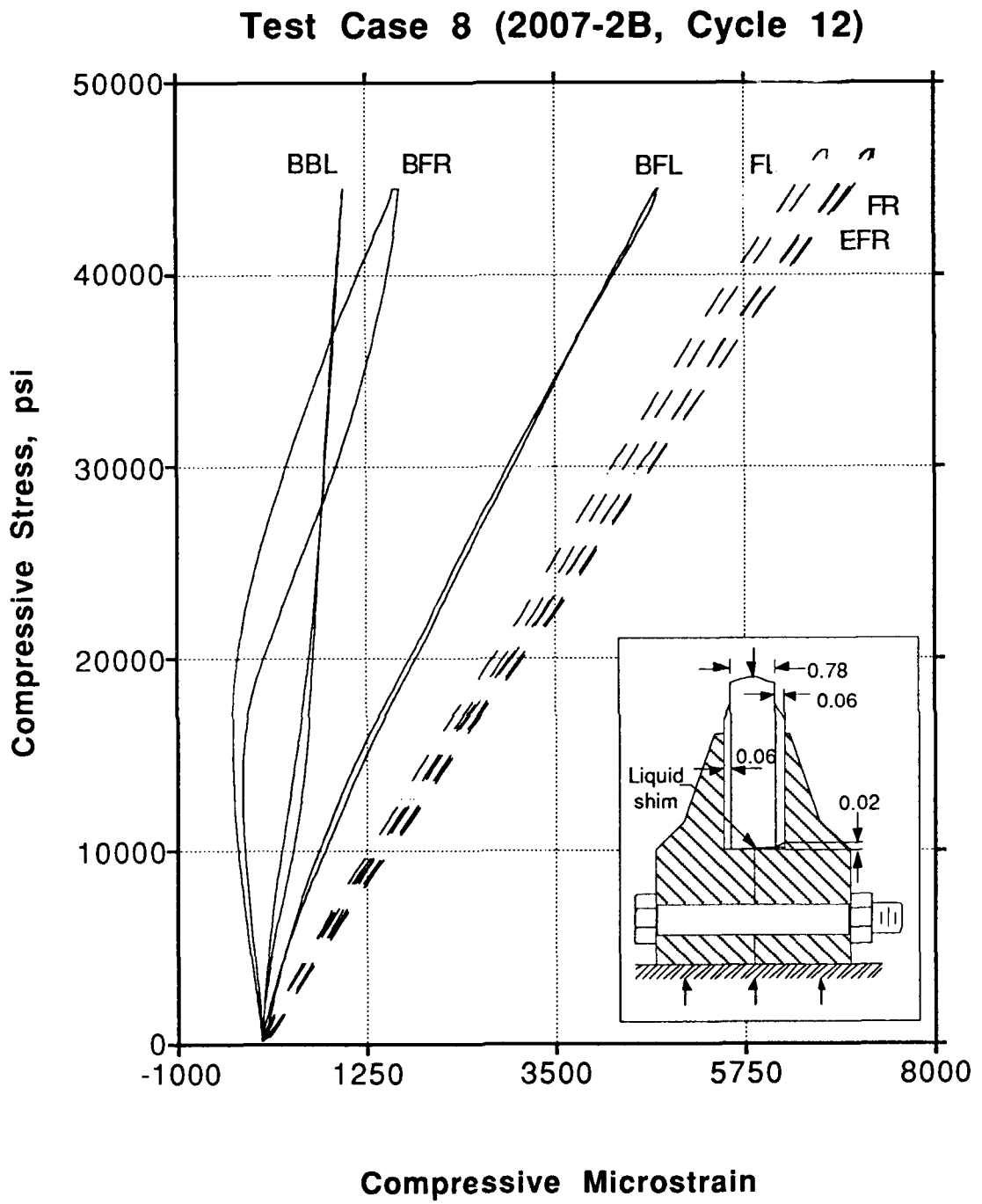


Figure 33 Compression Stress-Strain Curve for Cycle 12 of Test Case 8, Loading to 7000με.

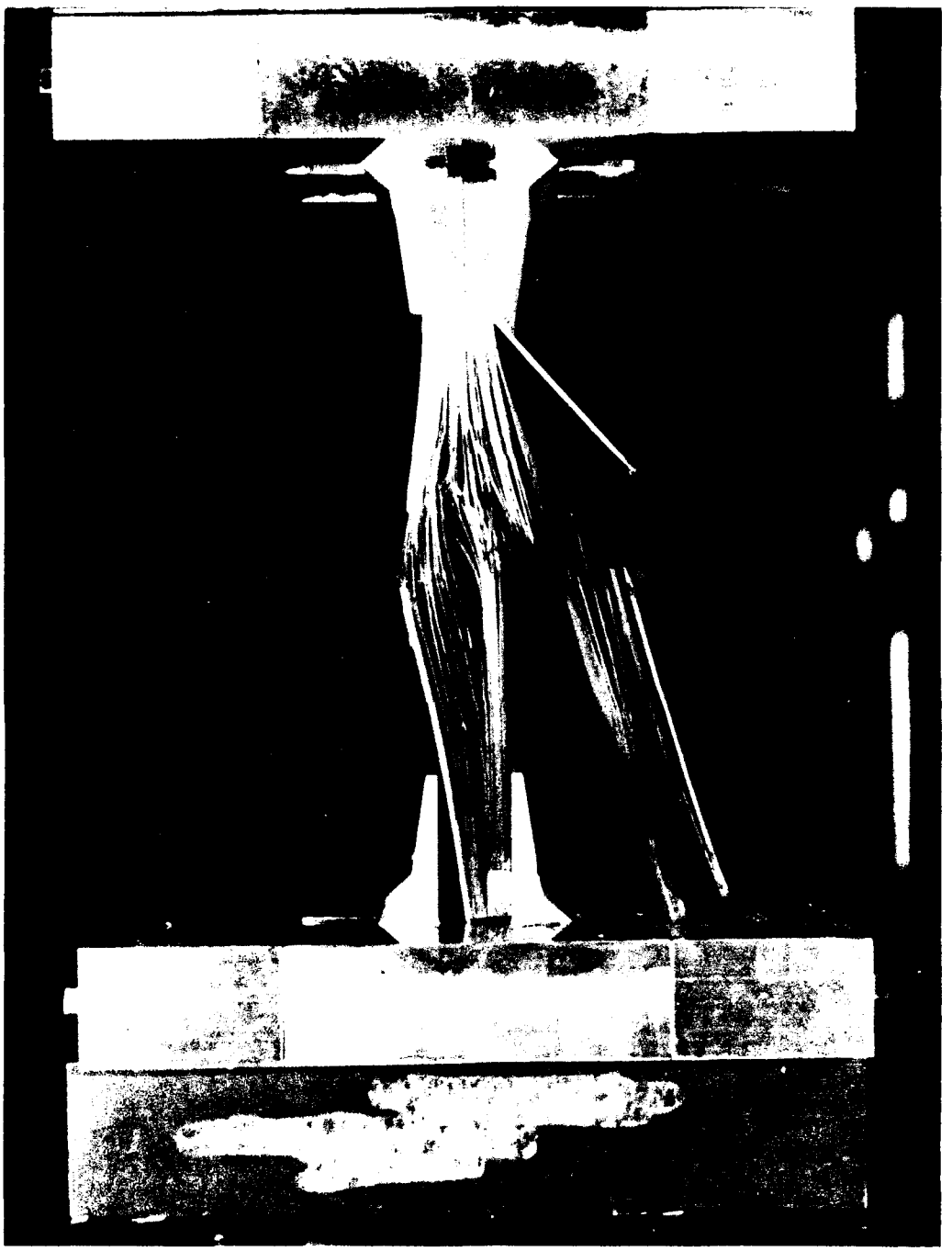

Figure 34 Photograph of Failed Specimen 2003-3 from Test Case 9.

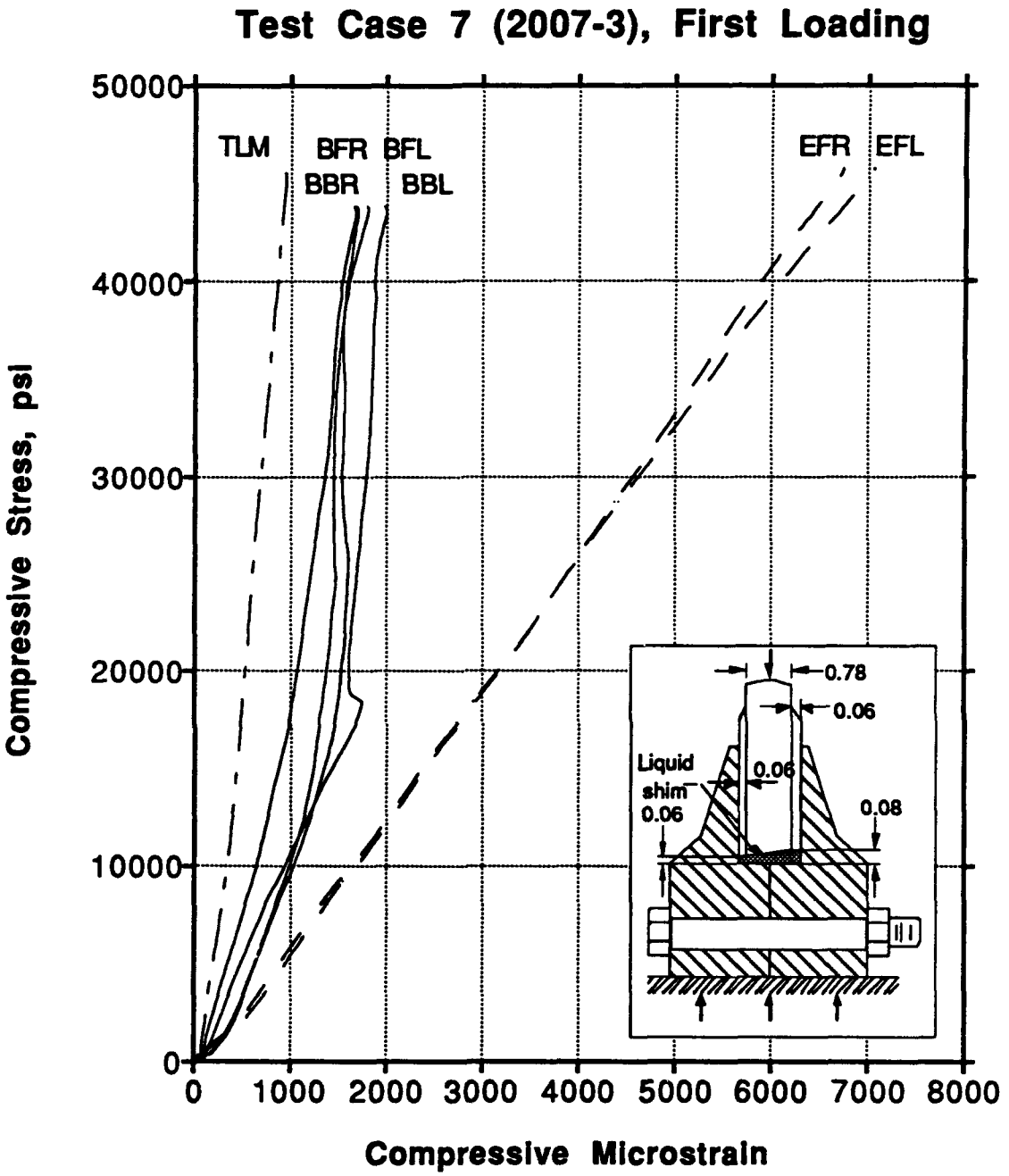


Figure 27 Compression Stress-Strain Curve for Test Case 7, 1st Loading, Spec. 2007-3.

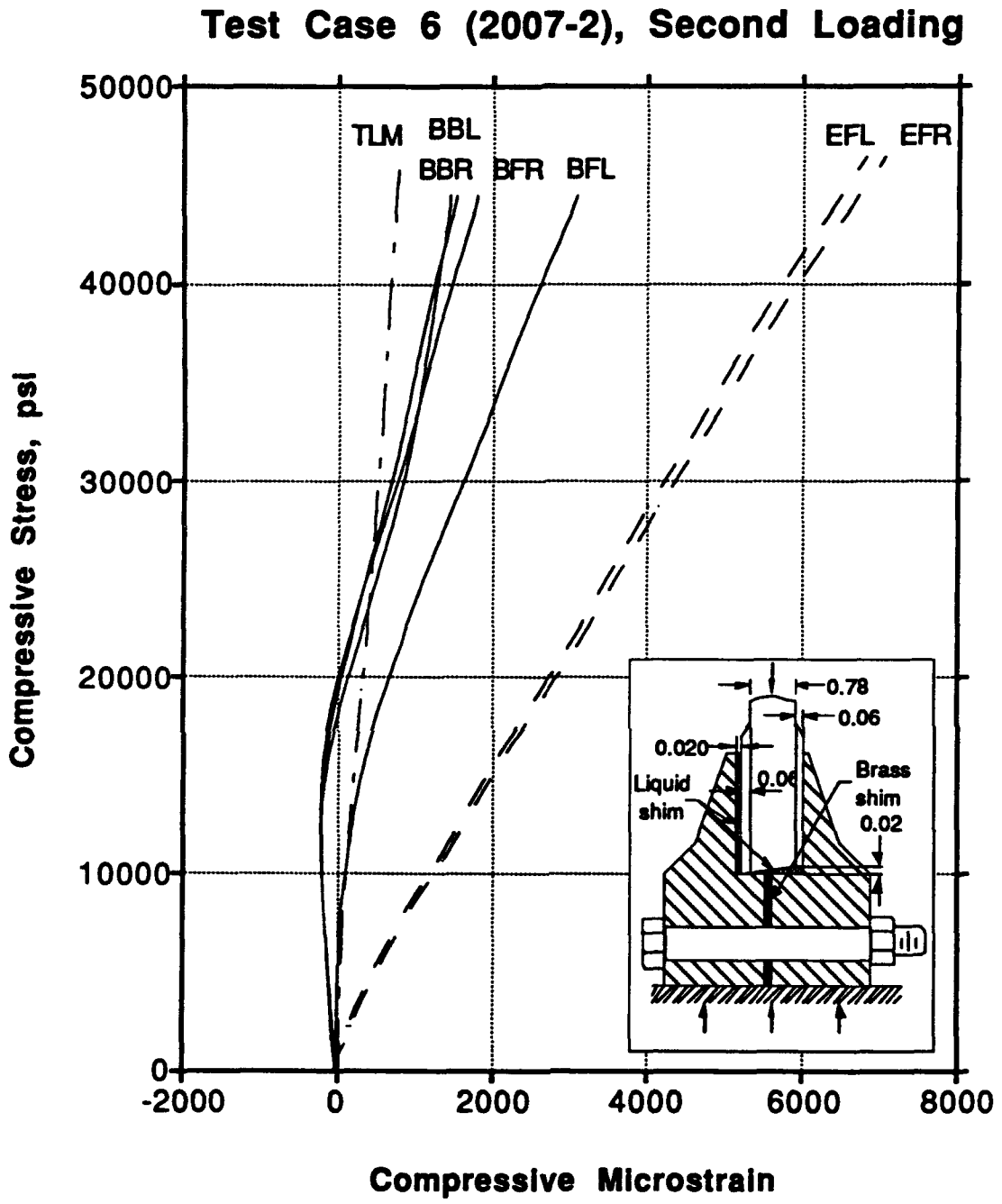


Figure 28 Compression Stress-Strain Curve for Test Case 6, 2nd Loading, Spec. 2007-2.

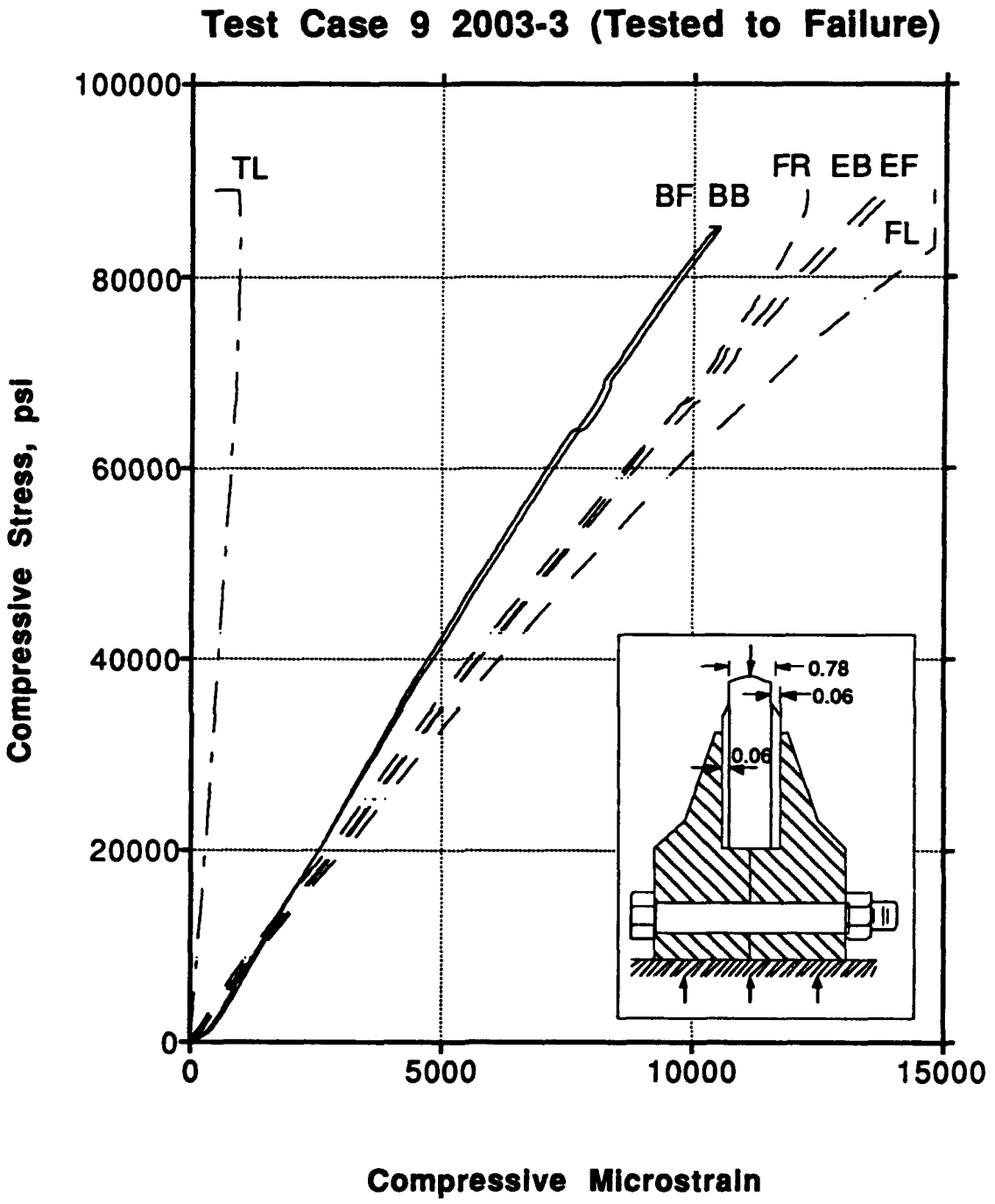


Figure 35 Compression Stress-Strain Curve for Test Case 9, Spec. 2003-3 Tested to Failure.

# Appendix A: Specimen and Fixture Dimensions

Table A1 Specimen Dimensions

| Specimen | Average S (in.) | Average W (in.) | Average Area ($in^2$) | Average T (in.) |
|---|---|---|---|---|
| 2003-1 | .8410 | 4.009 | 3.372 | .9599 |
| 2003-2 | .8387 | 4.007 | 3.361 | .9608 |
| 2003-3 | .8368 | 4.007 | 3.353 | .9596 |
| 2005 | .8358 | 4.003 | 3.346 | 1.0121 |
| 2007-1 | .8358 | 4.003 | 3.346 | .9609 |
| 2007-2 | .8416 | 4.001 | 3.367 | .9567 |
| 2007-3 | .8366 | 4.002 | 3.348 | .9610 |
| 2009 | .8411 | 4.004 | 3.368 | .9609 |

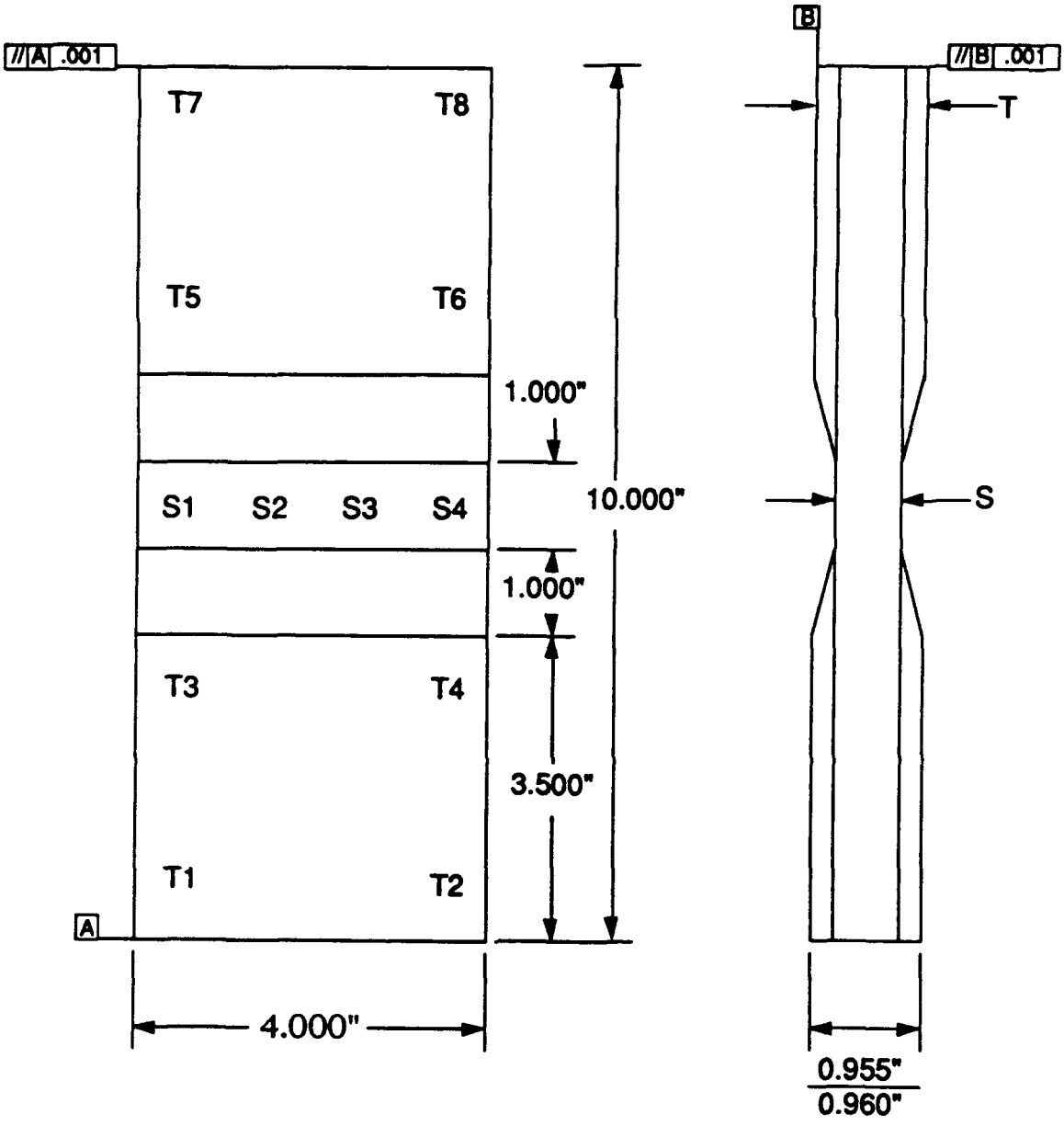
//A .001
T7
T8
T5
T6
1.000"
S1
S2
S3
S4
10.000"
1.000"
T3
T4
3.500"
T1
T2
A
4.000"
B
//B .001
T
S
0.955"
0.960"

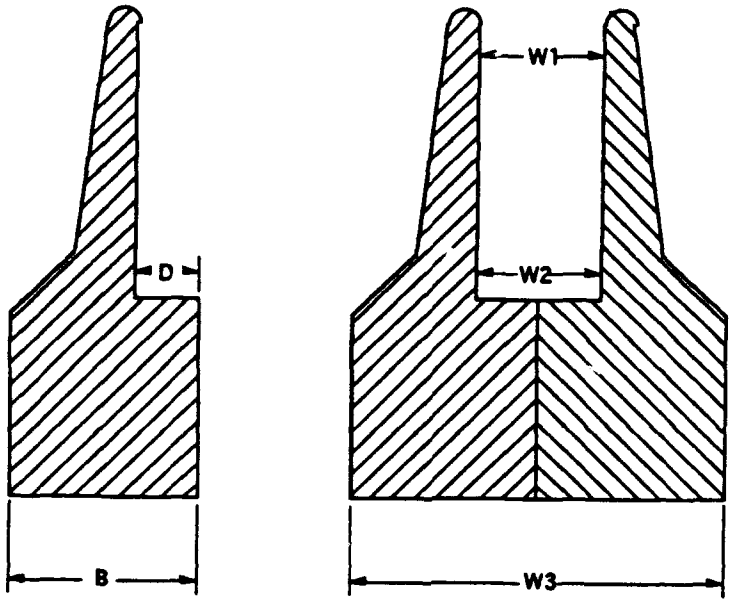


**Table A2 Fixture Dimensions**
**All measurements in inches.**

| Part # | B | D |
|---|---|---|
| 1 | 1.285 | 0.474 |
| 2 | 1.287 | 0.470 |
| 3 | 1.290 | 0.473 |
| 4 | 1.286 | 0.473 |
| 5 | 1.288 | 0.476 |
| 6 | 1.287 | 0.475 |
| 7 | 1.289 | 0.470 |
| 9 | 1.338 | 0.522 |
| 10 | 1.338 | 0.529 |
| 11 | 1.338 | 0.525 |

| Part # | W1 | W2 | W3 |
|---|---|---|---|
| 1-2 | 0.948 | 0.947 | 2.569 |
| 3-4 | 0.950 | 0.951 | 2.571 |
| 5-6 | 0.951 | 0.954 | 2.561 |
| 7-9 | 1.002 | 1.002 | 2.622 |
| 5-10 | 1.005 | 1.005 | 2.621 |
| 6-11 | 1.005 | 1.005 | 2.621 |

# Appendix B: Fixture Drawings

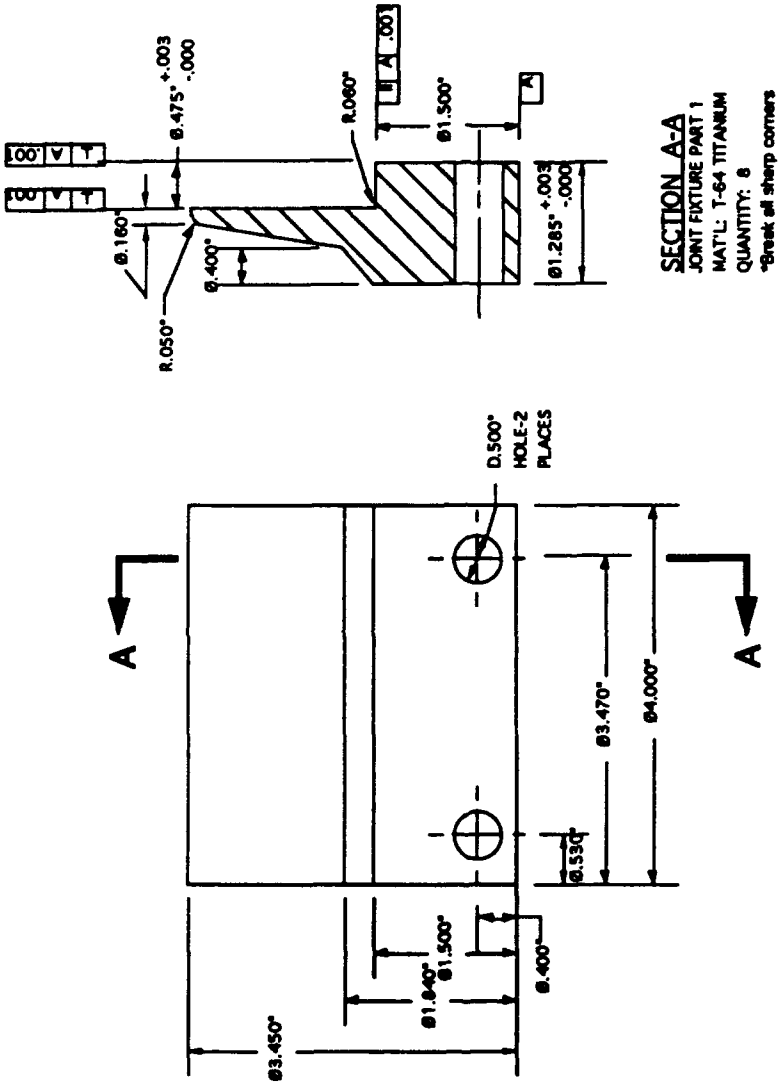
SECTION A-A
JOINT FIXTURE PART 1
MAT'L: T-64 TITANIUM
QUANTITY: 8
*Break all sharp corners
R.060"
Ø1.500"
Ø.475" +.003 -.000
Ø.160"
R.050"
Ø.400"
Ø1.285" +.003 -.000
D.500" HOLE-2 PLACES
Ø3.470"
Ø4.000"
Ø.530"
Ø1.500"
Ø1.840"
Ø.400"
Ø3.450"
A
A

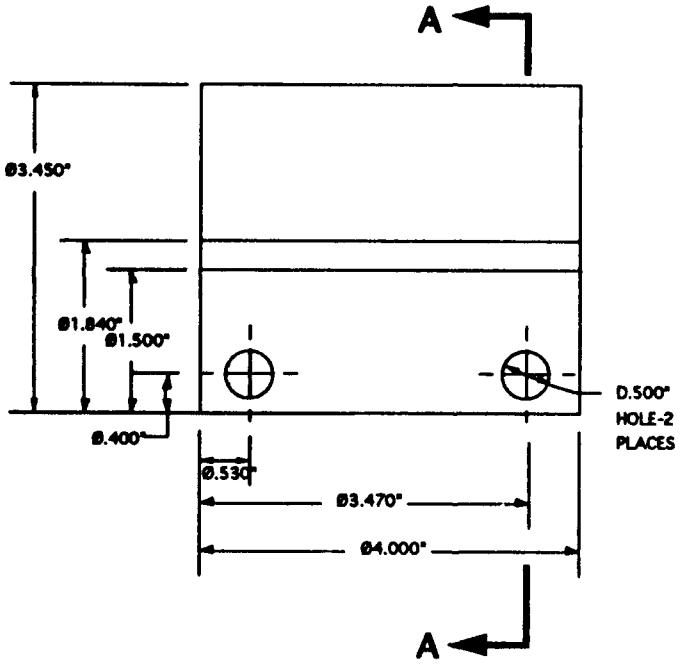


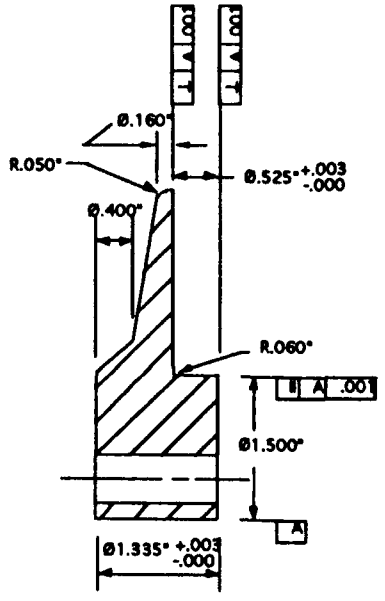


**SECTION A-A**
JOINT FIXTURE PART 2
MAT'L: T-64 TITANIUM
QUANTITY: 4
*Break all sharp corners

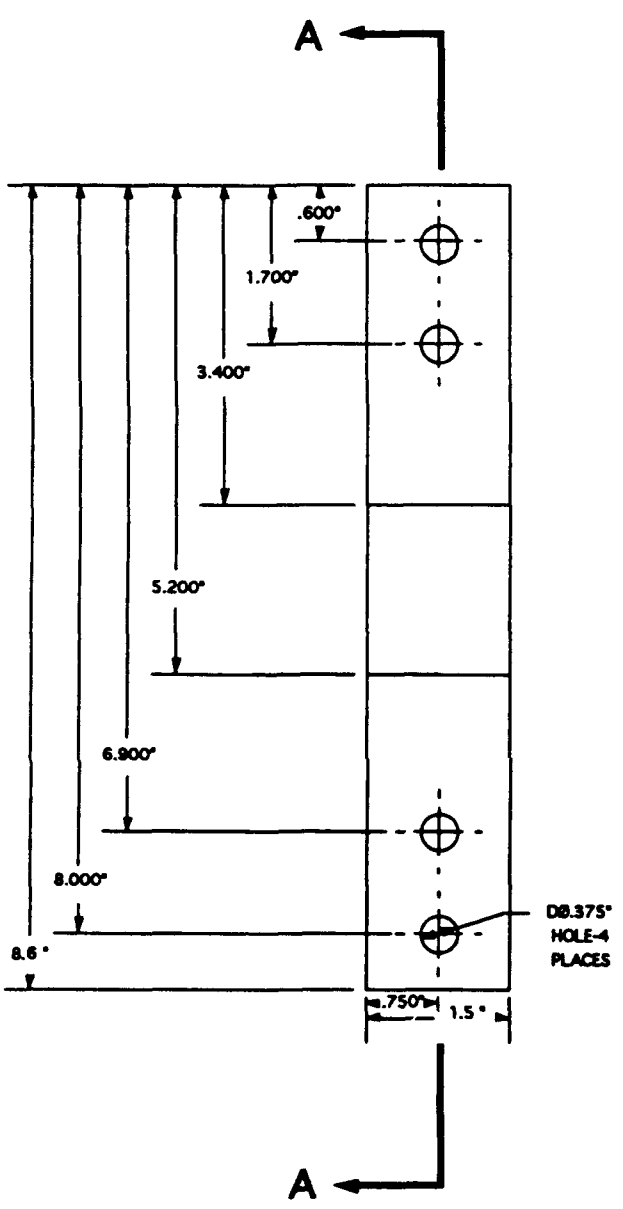


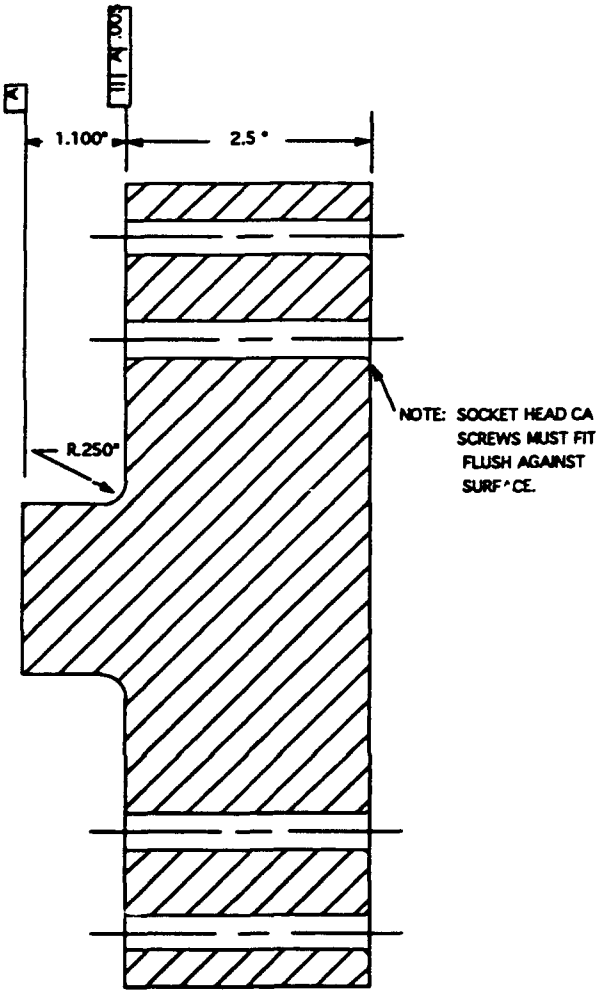


SECTION A-A
JOINT FIXTURE BASE PART 1
MAT'L: HY-130
QUANTITY: 2
*Break all sharp corners

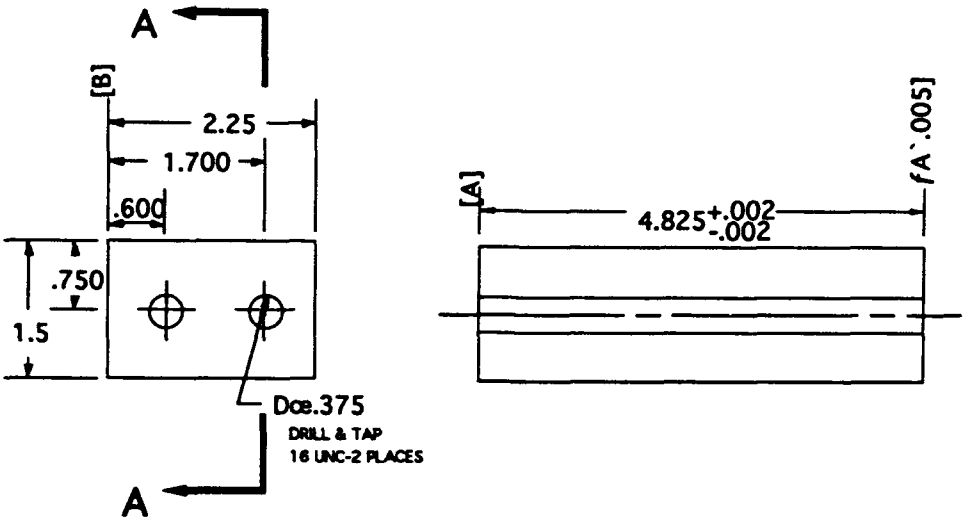


SECTION A-A
JOINT FIXTURE BASE PART 2
MAT'L: HY-130
QUANTITY: 2
*Break all sharp corners

NOTE: 1. ALL DIMENSIONS IN INCHES.
2. MARK/STAMP SURFACE B OF FINISHED PART.

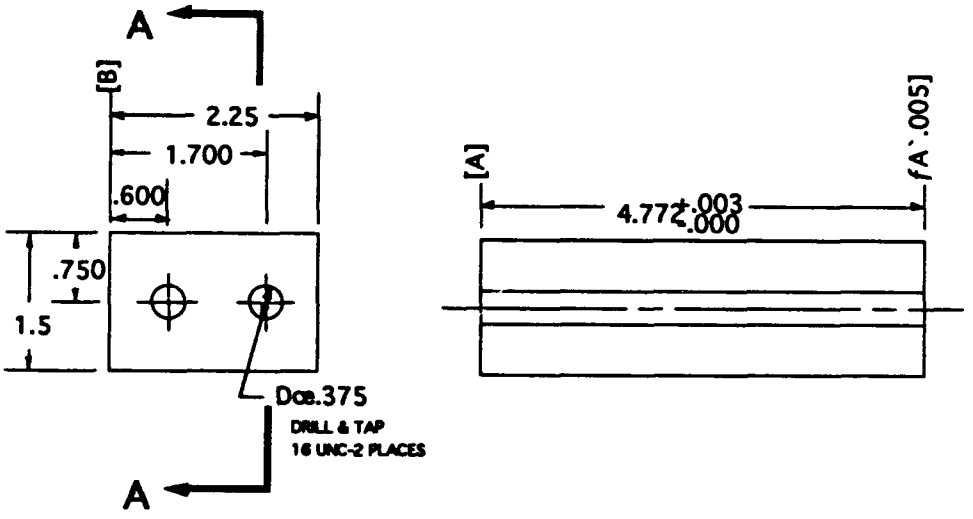


SECTION A-A
JOINT FIXTURE BASE PART 3
MAT'L: HY-130
QUANTITY: 2
*Break all sharp corners

NOTE: 1. ALL DIMENSIONS IN INCHES.
2. MARK/STAMP SURFACE B OF FINISHED PART.

# INITIAL DISTRIBUTION

Copies

12 DTIC

1 DARPA
1 (Kelly)

1 COMNAV Spec. War Com.
San DIego CA 92155
1 006 (Walker)

7 NAVSEA
1 05M3 (Pinto)
1 92R (Troffer)
1 92R (Spero)
1 55Y2 (McCarthy)
1 55Y2 (Will)
1 55Y2 (Nichols)
1 PMS 395 (Nyers)

3 NRL
1 6383 (Badaliance)
1 6383 (Wolock)
1 6385 (Chaskelis)

1 NSWC
1 R31 (Augl)

4 ONR
1 1132SM (Rajapakse)
1 1131S (Fishman)
1 1132SM (Barsoum)
1 1216 (Vasudevan)

1 ONT
1 233 (Remmers)

CENTER DISTRIBUTION

| Copies | Code | Name |
|---|---|---|
| 1 | 0115 | Caplan |
| 1 | 0112 | Douglas |
| 1 | 17 | Krenzke |
| 1 | 1702 | Corrado |
| 1 | 172 | Rockwell |
| 1 | 176 | Sykes |
| 5 | 1720.2 | Phyillaier |
| 1 | 1720.4 | Wiggs |
| 1 | 1730.2 | Critchfield |
| 1 | 2723 | Wilhelmi |
| 1 | 274 | Wang |
| 1 | 28 | Wacker |
| 10 | 2802 | Morton |
| 10 | 2802 | Camponeschi |
| 1 | 2803 | Cavallaro |
| 1 | 284 | Fischer |
| 1 | 2844 | Castelli |
| 1 | 522.2 | TIC (A) |
| 1 | 522.1 | TIC (C) |
| 1 | 5231 | Office Services |

INITIAL DISTRIBUTION (Continued)

2
IDA S&T Division
1801 N. Beauregard St.
Alexandria, VA, 22311
Attn. Mr. Charles Bersch
Attn. Mr. George Sorkin

Dr. R.E. Bohlmann
McDonnell Aircraft Company
Dept. 337, Bldg. 102 MC1021310
James S. McDonnell Blvd.
Berkely, MO 63134

Dr. Francis Chang
GD/Fort Worth Div, MZ 5984
PO Box 748
Fort Worth, TX 76101

Mr. Brian Coffenberry
ICI Composite Structures
2055 East Technology Circle
Tempe, AZ 85284

Mr. Richard Collins
Grumman Aircraft Systems
MS A01-10
Bethpage, NY 11714-3582

Dr. John Dugan, Jr.
Cortana Corp.
520 N. Washington St.
Falls Church, VA 22046

Mr. William Ferrara
CASDE Corp.
2300 Shirlington Rd.
Suite 600
Arlington, VA 22206

Dr. Don Flaggs
Mechanics and Materials Lab
Org 93-30 B/251
3251 Hanover St.
Palo Alto, CA 94304-1191

Dr. Chris Fortunko
NIST, Mail Code 430
325 South Broadway
Boulder, CO 80303

Mr. L.B. Greszczuk
McDonnell Space Systems Company
5301 Bolsa Avenue
Hunington Beach, CA 92647

Ms. Tricia Hankinson
PRC, Inc.
1555 Wilson Blvd., Suite 600
Arlington, VA 22209

Mr. Jeffrey D. Hendrix
Hercules Aerospace Co.
1800 K Street NW, Suite 710
Washington, DC 20006

Ms. Diana Holdinghausen
McDonnell Aircraft Company
D357, MC 1021310
PO Box 516
St. Louis, MO 63166

Mr. Pete Hoffman
McDonnell Aircraft Company
D357, MC 1021310
PO Box 516
St. Louis, MO 63166

Dr. Dan King
McDonnell Aircraft Company
MC1021310
PO Box 516
St. Louis, MO 63166

Mr. Steve Kopf
EI DuPont DeNemours & Co.
Composites Div.
Chestnut Run Plaza
Box 80702
Wilmington, DE 19880-0702

Mr. G. Leon
General Dynamics, EB DIv.
Dept. 442, Station J11-431
Eastern Pt. Rd.
Groton, CT 06340

Mr. R. E. Lovejoy
Coastal Systems Station
Code 30E
Panama City, FL 32407-5000

Mr. John MacKay
Touchstone Research Laboratory
The Millennium Centre
Triadelphia, WV 26059

Dr. Ralph Nuismer
Hercules Composite Structures
Mail Stop X11K4
PO Box 98
Magna, UT 84044-0098

Mr. Jim Suarez
Grumman Aircraft Systems
MS B44/35
Bethpage, NY 11714-3582

Mr. Thomas Triplett
ICI Composite Structures
2055 East Technology Circle
Tempe, AZ 85284

Mr. Charles Zanis
CASDE Corporation
2800 Shirlington Road
Suite 600
Arlington, VA 22206

Dr. Mohamed G. Abdallah
Hercules Incorporated
Science and Technology Dept.
Bacchus Works
Magna, UT 84044-0098

Dr. Don Adams
ME Dept.
Univ. of Wyoming
Laramie, WY 82071

Dr. T. Bogetti
Mechanics and Structures Branch
U.S. BRL
Aberdeen, MD 21005-5066

Dr. John H. Bode
Alliant Techsystems
7225 Northland Drive
Brooklyn Park, MN 55428

Anthony A. Caiazzo, P.E.
Materials Sciences Corp.
930 Harvest Drive
Union Meeting Corp. Center
Blue Bell, PA 19422

Douglas S. Cairns, Ph.D.
Hercules Incorporated
Science & Technology Department
Bacchus Works
Magna, UT 84044-0098

Dr. Reaz Chaudhuri
Dept. of Civil Eng.
3220 Merrill Eng. Bldg.
Univ. of Utah
Salt Lake City, UT 84112

Dr. David Cohen
Hercules Aerospace Company
Missiles, Ordnance & Space Group
Bacchus Works
Magna, UT 84044-0098

Dr. Elizabeth Geoke
U.S AMTL, Attn. SLCMT-MRM
405 Arsenal Street
Watertown, MA 02172-0001

John W. Gillespie, Jr., Ph.D.
Center for Composite Materials
Composites Manufacturing Science
Laboratory
University of Delaware
Newark, DE 19716

Dr. Bob Green
Director, CNDE
102 Maryland Hall
The Johns Hopkins Univ.
Baltimore MD, 21218

Dr. Jeff Hall
General Dynamics, EB DIv.
Dept. 442, Station J11-431
Eastern Pt. Rd.
Groton, CT 06340

2
L. J. Broutman & Assoc. Ltd.
3424 South State St.
Chicago, IL 60616
Attn. K. E. Hofer
Attn. Mr. Gregory N. Skaper

Dr. Donald L. Hunston
Polymer Composites Group
Polymers Division
NIST
Building 224, Room A209
Gaithersburg, MD 20899

Mr. Paul Miller
Newport News Shipbuilding
& Drydock Company
San Diego Office
1550 Hotel Circle, N.
Suite 400
San Diego, CA 92108

Robert Pasternak
US AMTL
Attn. SLCMT-MRM
Watertown, MA 02172-0001

Prof. D. Pecknold
Dept. of Civil Eng., Univ. of IL
3129 Newmark Lab
205 N. Mathews
Urbana , IL 61801

Vasilios Peros
Martin Marietta
Aero & Naval Systems
103 Chesapeake Park Plaza
Baltimore, MD 21220

Prof. Dick Schapery
Dept. of Aerospace Eng.
& Eng. Mechanics
Univ. of Texas
Austin, TX 78712

Dr. R Sierakowski
Chairman, Civil Eng. Dept.
Ohio State Univ.
2070 Neil Ave.
470 Hitchcock Hall
Columbus, OH 43210

K. A. Stubenhofer
Information Center
Lord Corp.
PO Box 10039
Erie, PA 16514

Prof. A. J. Vizzini
The University of Maryland
College of Engineering
Department of Aerospace Eng.
College Park, MD 20742

Mr. John M. Winter, Jr.
CNDE
102 Maryland Hall
The Johns Hopkins University
Baltimore, MD 21218

Prof. Michael Wisnom
Dept. of Aerospace Engineering
University of Bristol
Queens Bldg., Univ. Walk
Bristol, BS8 1TR

Dr. Fuh-Gwo Yuan
Department of Mechanical
& Aerospace Engineering
North Carolina State University
Raleigh, NC 27695-7910